REGENERATION

PTMA controls cardiomyocyte proliferation and cardiac repair by enhancing STAT3 acetylation

Ning Liu[1]†, Jianqiu Pei[2]†, Yifan Xie[1]†, He Xuan[1], Nan Jiang[3], Jue Wang[3], Yangyang Gao[4], Yixun Li[1], Xiangjie Li[1], Weijing Liu[1], Chenying Xiang[1], Zheng Qiao[1], Haiping Cao[5], Yu Nie[1,6]*

The adult mammalian heart has limited regenerative capacity due to the low proliferative ability of cardiomyocytes, whereas embryonic cardiomyocytes exhibit robust proliferative potential. Using single-cell RNA sequencing of embryonic hearts, we identified prothymosin α (PTMA) as a key factor driving cardiomyocyte proliferation. Overexpression of PTMA in primary mouse and rat cardiomyocytes significantly promoted cardiomyocyte proliferation and similarly enhanced proliferation in human iPSC–derived cardiomyocytes. Conditional knockout of *Ptma* in cardiomyocytes impaired neonatal heart regeneration. AAV9-mediated overexpression of *Ptma* extended the neonatal proliferative window and showed therapeutic promise for enhancing adult heart regeneration. Mechanistically, PTMA interacted with MBD3, inhibiting its deacetylation activity within the MBD3/HDAC1 NuRD complex. This inhibition increased STAT3 acetylation, which positively regulated STAT3 phosphorylation and activation of its target genes. These findings establish PTMA as a critical regulator of heart regeneration and suggest its potential as a therapeutic target for ischemic myocardial injury.

INTRODUCTION

Ischemic heart disease continues to be a leading cause of mortality worldwide, posing a substantial threat to human health (*1*). Ischemic stress leads to extensive cardiomyocyte death, which consequently overburdens the surviving cells. Due to the limited proliferative capacity of adult cardiomyocytes, the heart cannot adequately repair itself after myocardial infarction (MI) (*2*). This initiates a cascade of pathological cardiac remodeling that can culminate in the progression to heart failure (*3*, *4*). In stark contrast, embryonic cardiomyocytes have a potent proliferative capacity that is crucial for driving embryonic heart growth and ensuring normal heart development (*5*, *6*). The embryonic heart can accomplish complete regeneration even tolerating a loss of 50 to 60% cardiomyocytes, through augmenting the resident cardiomyocyte proliferation (*7*). However, this regenerative ability rapidly declines shortly after birth (*8*–*11*). It is hypothesized that the silencing of embryonic proliferation activators marks the cardiomyocyte cell cycle arrest. Therefore, identifying the key molecules that enhance embryonic cardiomyocyte proliferation could unlock critical targets for promoting adult cardiac regeneration.

To uncover the pivotal genes that govern cardiomyocyte proliferation, we performed single-cell RNA sequencing (scRNA-seq) on embryonic hearts across a range of developmental stages [embryonic day 8.5 (E8.5) to E17.5]. By integrating these data with RNA sequencing (RNA-seq) from cardiomyocytes at different postnatal ages and conducting functional validation, we identified *Ptma* as a core driver of cardiomyocyte proliferation. Prothymosin α (PTMA) is a nuclear protein encoded by *Ptma*, which plays a pivotal role in numerous cellular processes, including cell division, chromatin remodeling and apoptosis (*12*–*17*). However, the specific role and underlying mechanisms of nuclear PTMA in promoting cardiomyocyte proliferation and heart regeneration remain to be further elucidated.

In this study, we demonstrated that *Ptma* was a core conserved gene that drove the proliferation of primary cardiomyocytes from mice and rats, as well as human-induced pluripotent stem cells. Our investigation further confirmed that PTMA was both necessary and sufficient for promoting heart regeneration and functional repair in both neonatal and adult mice. Additionally, we elucidated that PTMA facilitated cardiomyocyte proliferation through interacting with MBD3, which suppressed the deacetylation activity of HDAC1 in the nucleosome remodeling and deacetylation repressor (NuRD) complex, thereby promoting signal transducer and activator of transcription 3 (STAT3) acetylation and phosphorylation activation. Our findings demonstrated that PTMA could serve as a promising therapeutic target for enhancing adult cardiac repair, opening a groundbreaking therapeutic avenue for patients suffering from ischemic heart disease.

RESULTS

scRNA-seq of embryonic hearts reveals *Ptma* as a key factor driving cardiomyocyte proliferation

To identify key factors driving proliferation in embryonic cardiomyocytes, we performed scRNA-seq on cardiac cells from seven developmental stages, including E8.5, E9.0, E9.5, E10.5, E11.5, E14.5, and E17.5 (Fig. 1A), and this enables a detailed exploration of the dynamic changes in gene expression that underpin the embryonic cardiomyocyte development. We captured and sequenced 36,039 cells across all samples, achieving a median of 3880 genes and 16,249 unique transcripts per cell after quality filtering (fig. S1, A and B). We visualized the integrated dataset using a *t*-distributed stochastic neighbor embedding (*t*-SNE) plot with respect to cell types and their time points (Fig. 1B and fig. S1C). Using the expression of known cellular marker genes and distinct gene expression signatures, we

[1]State Key Laboratory of Cardiovascular Disease, Fuwai Hospital, National Center for Cardiovascular Disease, Chinese Academy of Medical Sciences and Peking Union Medical College, Beijing 100037, China. [2]Department of Biochemistry and Molecular Biology, School of Basic Medical Sciences, Capital Medical University, Beijing 100069, China. [3]The First School of Clinical Medicine, Wenzhou Medical University, Wenzhou 325000, China. [4]Xi'an International Medical Center, Xi'an 710000, China. [5]Department of Cardiology, Nanchong Central Hospital, Nanchong 637000, China. [6]National Health Commission Key Laboratory of Cardiovascular Regenerative Medicine, Fuwai Central-China Hospital, Central China Branch of National Center for Cardiovascular Diseases, Zhengzhou 450046, China.
*Corresponding author. Email: nieyuniverse@126.com, nieyu@fuwaihospital.org
†These authors contributed equally to this work.

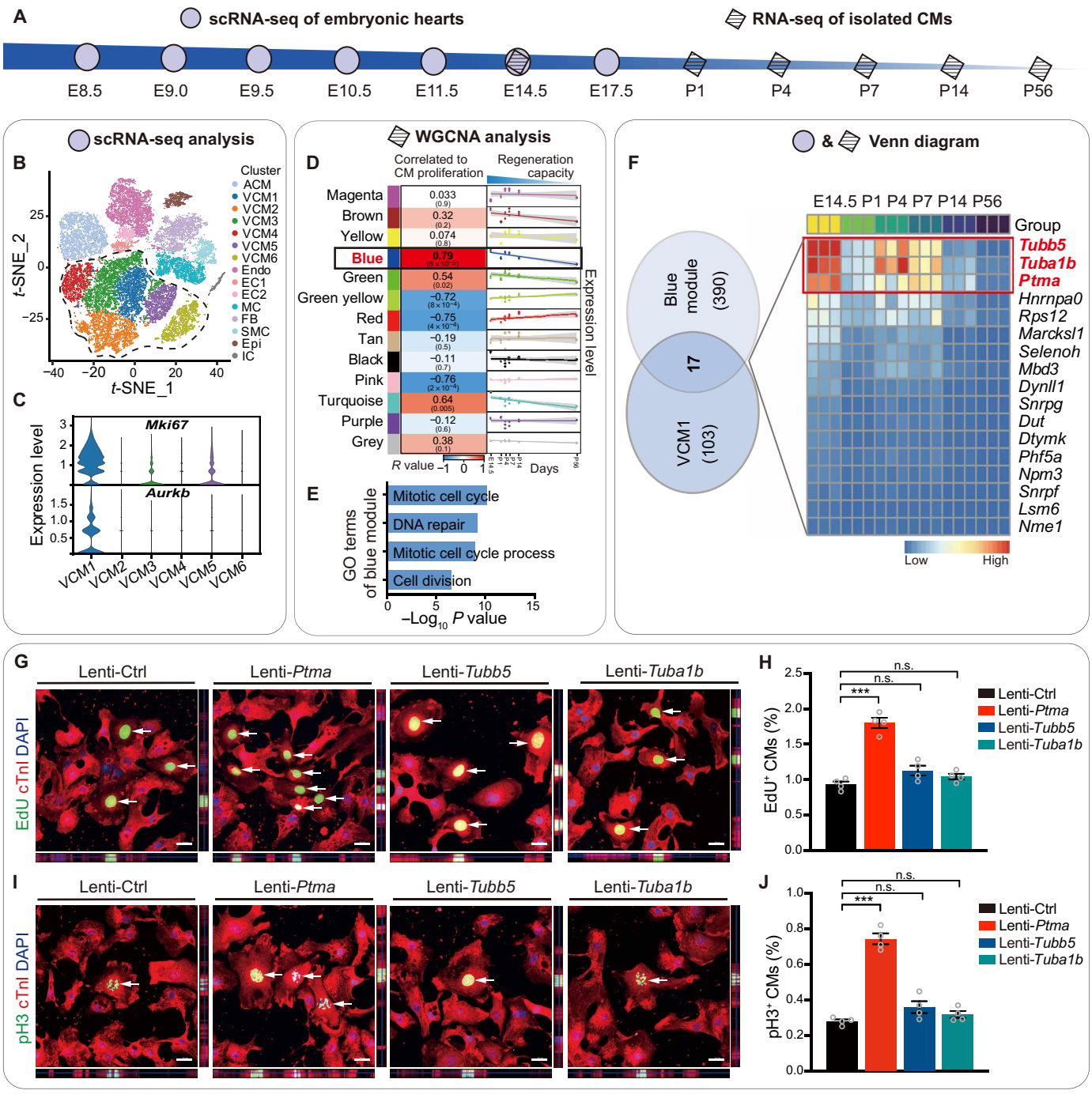

Fig. 1. scRNA-seq of embryonic hearts reveals *Ptma* as a key factor driving cardiomyocyte proliferation. (**A**) Schematic of the experimental design for screening cardiomyocyte proliferative factors. (**B**) The *t*-distributed stochastic neighbor embedding (*t*-SNE) visualization of the 15 clusters in embryonic hearts (n = 36,039 cells). ACM, atrial cardiomyocytes; VCM, ventricular cardiomyocytes; Endo, endocardial cells; EC, endothelial cells; MC, mesenchymal cells; FB, fibroblasts; SMC, smooth muscle cells; Epi, epicardial cells; IC, immune cells. (**C**) Violin plots of the expression of cell cycle gene *Mki67* and *Aurkb* in VCM1-VCM6 cells. (**D**) Heatmap of the relationship between the blue module and cardiomyocyte proliferation traits (left), and scatter plot (right) presenting the module gene expression pattern in various stages of cardiomyocyte development. The correlation coefficients (r) values and the corresponding P values are shown in the rectangles and the brackets, respectively. (**E**) Gene Ontology (GO) terms of the blue module. (**F**) Venn diagram presenting the intersection of differential expressed genes in VCM1 and hub genes in the blue module (left), and the heatmap presenting the expression of 17 co-expressed genes in cardiomyocytes at differential heart developmental periods (right). (**G** to **J**) Representative images of EdU incorporation (G), pH3 (I) staining in neonatal mouse cardiomyocytes (NMCMs) infected with lenti-*Ptma*, lenti-*Tubb5*, and lenti-*Tuba1b*. Scale bars, 20 μm. Quantification of EdU (H)– and pH3 (J)–positive cardiomyocytes, n = 4. Data are presented as means ± SEM. By One-way analysis of variance (ANOVA) analysis, ***$P < 0.001$ (versus lenti-Ctrl); n.s. indicates that the P value is not significant. DAPI, 4′,6-diamidino-2-phenylindole.

identified the major cardiac cell types (fig. S1, D and E), including six ventricular cardiomyocyte clusters (VCM1 to VCM6) (Fig. 1B and fig. S1F). Among the six ventricular cardiomyocyte clusters, VCM1 highly expressed cell cycle genes, such as *Mki67* and *Aurkb* (Fig. 1C and fig. S1, G to L). The cell-cycle scoring analysis (*18*) showed that 78.39% of VCM1 cardiomyocytes were in the G_2-M phase, while the other five clusters exhibited lower proportions (fig. S1M), indicating that VCM1 is the proliferative cardiomyocyte population during embryonic heart development. Then, we conducted differential gene expression analysis by comparing VCM1 with the other five VCM clusters and identified 120 genes [fold change (FC) > 1.2, adjusted *P* value < 0.05] that were highly expressed in over 90% of VCM1 cardiomyocytes (Fig. 1F).

To focus on genes that regulate the proliferation of cardiomyocytes during both embryonic and postnatal stages, we used our previous bulk RNA-seq data of isolated cardiomyocytes from regenerative E14.5 and neonatal hearts [postnatal day 1 (P1), P4, and P7], along with the nonregenerative adolescent (P14) and adult (P56) hearts (*19*). We conducted weighted gene co-expression network analysis (WGCNA) (*20*) and identified a gene module consisting of 407 hub genes [module membership (MM) > 0.95, gene significance (GS) > 0.75, adjusted *P* value < 0.05], whose expression pattern correlates with cardiomyocyte proliferation window [correlation coefficient (r) = 0.79, *P* value = 8.0×10^{-5}] (Fig. 1, A and D to F, and fig. S1N). Combined analysis revealed that, among the highly expressed genes in VCM1, 17 genes were down-regulated in conjunction with the loss of cardiomyocyte proliferative capacity during postnatal heart development, among which *Ptma*, *Tubb5*, and *Tuba1b* were the most significant (Fig. 1F and figs. S1O and S2A).

We overexpressed *Ptma*, *Tubb5*, and *Tuba1b*, respectively, in primary neonatal mouse cardiomyocytes (NMCMs) using lentivirus to investigate whether these genes induce cardiomyocyte proliferation (fig. S2, B and C). 5-Ethynyl-2′-deoxyuridine (EdU) incorporation and immunostaining of phospho–histone H3 (pH3; a marker of mitosis) showed that only PTMA overexpression significantly enhanced both cardiomyocyte DNA synthesis and mitosis (Fig. 1, G to J). To further investigate the relevance of PTMA in embryonic cardiomyocyte proliferation, we performed co-immunofluorescence staining for PTMA, cardiomyocyte marker cTnT, and the cell cycle marker Ki67. Our analysis revealed that 94.85 ± 1.84% of PTMA-positive cardiomyocytes were also Ki67 positive, whereas only 10.90 ± 3.54% of PTMA-negative cardiomyocytes exhibited Ki67 positivity (fig. S2, D and E). These findings strongly suggest that PTMA is a core factor driving cardiomyocyte cell cycle reentry in embryonic hearts.

PTMA promotes postnatal and adult cardiomyocyte proliferation in vivo

To investigate whether PTMA overexpression induces cardiomyocyte proliferation at the early postnatal stage, we constructed an adeno-associated virus 9 (AAV9) vector with a cTnT promoter for cardiomyocyte-specific overexpression of *Ptma* (AAV9-*Ptma*) (*21*). We then infected the wild-type (WT) mice with AAV9-*Ptma* at P1, and AAV9-*Luciferase* (AAV9-*Luc*)–infected hearts were used as negative control. Four days after AAV9 infection, we labeled the cardiomyocytes with EdU every day for 4 days by intraperitoneal injection. We performed immunofluorescence co-staining for cTnT with proliferative markers EdU, pH3, and Aurora B in P8 hearts (Fig. 2A). The results showed that PTMA overexpression elevated the proportion of EdU-positive cardiomyocytes from 4.07 ± 0.97% to 16.73 ± 1.16% (Fig. 2, B and C). Additionally, PTMA overexpression enhanced the number of cardiomyocytes undergoing mitosis, with the proportion of pH3-positive cardiomyocytes increasing from 2.09 ± 0.16% in AAV9-*Luc* hearts to 5.73 ± 0.77% in AAV9-*Ptma* hearts (Fig. 2, D and E). Of note, PTMA overexpression hearts exhibited a 4.86-fold increase in Aurora B–positive cardiomyocytes, rising from 0.022 ± 0.001% to 0.107 ± 0.030% (Fig. 2, F and G). These findings clearly indicate that PTMA overexpression effectively promotes cardiomyocyte cell cycle reentry during the early postnatal stage.

To further investigate whether PTMA is sufficient to promote adult cardiomyocyte proliferation, we overexpressed PTMA in the adult hearts by intramyocardial injection of AAV9-*Ptma* or AAV9-*Luc*. Four days after AAV9 injection, we labeled the cardiomyocytes with EdU daily through intraperitoneal injection (Fig. 2H). Immunostaining showed that PTMA overexpression led to a substantial increase in adult cardiomyocyte DNA synthesis (EdU^+; Fig. 2, I and J), mitosis ($pH3^+$; Fig. 2, K and L), and cytokinesis (Aurora B^+; Fig. 2, M and N). Collectively, these comprehensive results demonstrate that overexpression of PTMA is sufficient to promote cardiomyocyte cell cycle reentry in adult mice.

Ptma is required for cardiomyocyte proliferation and heart regeneration

To further explore the role of PTMA in cardiomyocyte proliferation, we isolated cardiomyocytes from E17.5 mouse hearts and infected them with an adenovirus carrying a green fluorescent cell cycle reporter system (FUCCI) (*22*). This system overexpresses a nonfunctional human Geminin deletion mutant fused to Azami Green [mAG-hGeminin (1/110)], driven by the troponin T2 (Tnnt2) promoter, to specifically label cardiomyocytes in the S, G2, and M phases of the cell cycle. We knocked down *Ptma* in cardiomyocytes with small interfering RNA (siRNA; si-*Ptma*) (fig. S3, A and B) and observed a significant decrease in the proportion of FUCCI-labeled cardiomyocytes compared with scrambled siRNA (si-NC) (Fig. 3, A and B). We also observed a significant decrease in EdU^+, $pH3^+$, and Aurora B^+ cardiomyocytes following si-*Ptma* treatment both in E17.5 and P1 hearts (fig. S3, C to H). RNA-seq and the following quantitative reverse transcription polymerase chain reaction (qRT-PCR) revealed that *Ptma* knockdown down-regulated genes associated with cardiomyocyte cell cycle and cell division (fig. S3, I and J). These results suggest that *Ptma* is essential for cardiomyocyte proliferation.

We then generated cardiomyocyte–conditional knockout mice by crossing Myh6-Cre mice with $Ptma^{fl/fl}$ mice (*Ptma*-cKO mice) and performed apical resection (AR) operation at P1 (Fig. 3C). Immunostaining of PTMA protein showed effective knockout of *Ptma* in cardiomyocytes with no effect on the expression of PTMA in non-cardiomyocytes in *Ptma*-cKO hearts (Fig. 3, D and E). We collected the injured hearts at 7 days post-resection (dpr). Compared to $Ptma^{fl/fl}$ littermates, we observed a significant reduction in EdU^+, $pH3^+$, and Aurora B^+ cardiomyocytes in *Ptma*-cKO hearts (Fig. 3, F to K). Wheat germ agglutinin (WGA) staining indicated that *Ptma* deficiency leads to an increase in cardiomyocyte size (Fig. 3, L and M). Masson's staining showed that the heart regeneration capacity was suppressed in *Ptma*-cKO mice, with a significant increase in the fibrotic area and a decrease in the number of regenerative hearts at 1 month post–AR injury (Fig. 3, N to P). Echocardiography revealed a reduction in cardiac ejection fraction (EF) and left ventricular

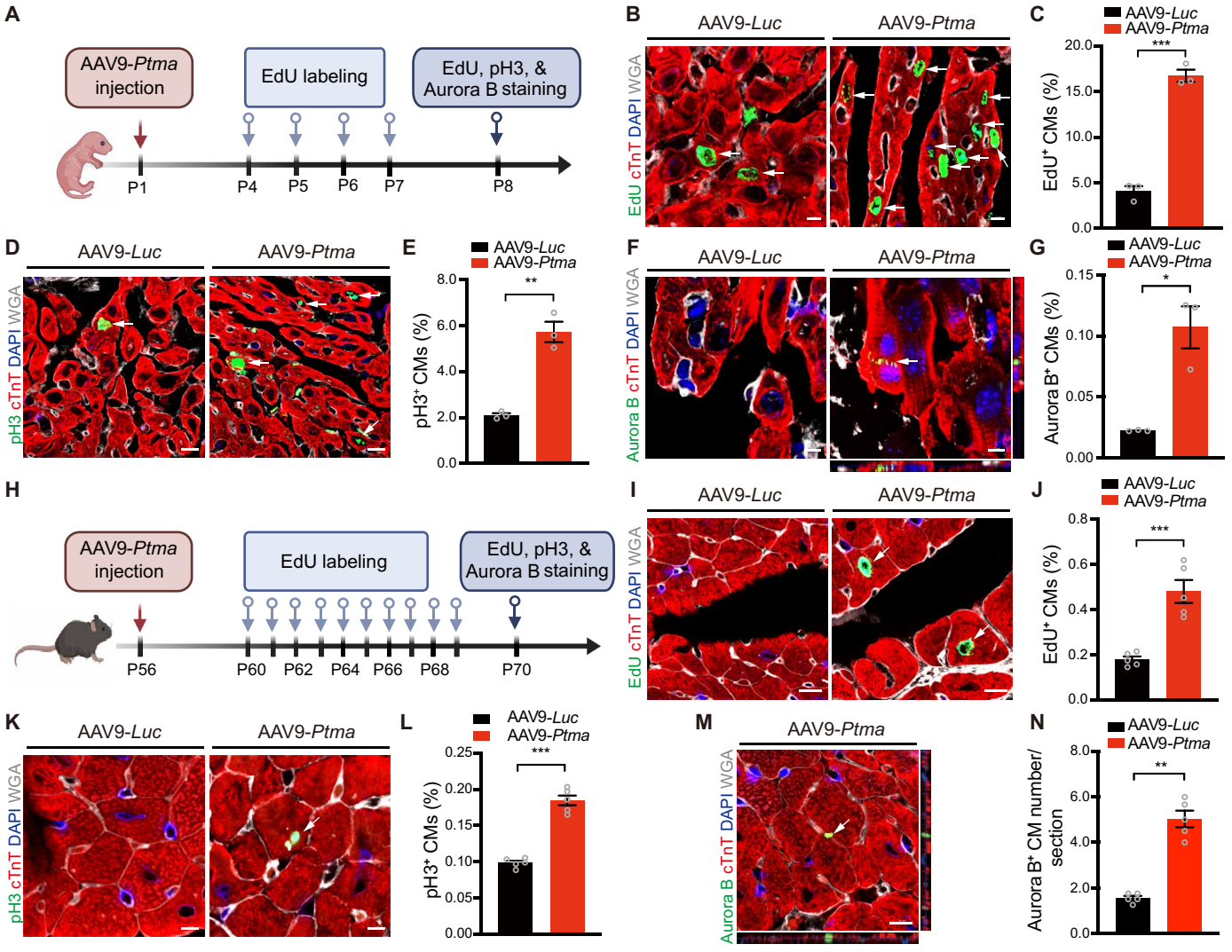

Fig. 2. PTMA promotes postnatal and adult cardiomyocyte proliferation in vivo. (**A**) Schematic plot showing the experimental procedure for AAV9-delivered PTMA overexpression in neonatal hearts, created in BioRender (S. Gai, 2025), https://BioRender.com/q64z784, with modifications. (**B** to **G**) Representative images of immunostaining for EdU (B), pH3 (D), and Aurora B (F) heart sections. Scale bars, 5 μm [(B) and (F)] and 10 μm (D). Quantitative analysis of EdU (C)–, pH3 (E)–, and Aurora B (G)–positive cardiomyocytes at P8 mice hearts, $n = 3$. Data are presented as means ± SEM, by Student's t test, $^{*}P < 0.05$, $^{**}P < 0.01$, and $^{***}P < 0.001$. (**H**) Schematic plot showing the experimental procedure for AAV9-delivered PTMA overexpression in adult hearts, created in BioRender (S. Gai, 2025), https://BioRender.com/q64z784, with modifications. (**I** to **N**) Representative images of immunostaining for EdU (I), pH3 (K), and Aurora B (M) heart sections. Scale bars, 10 μm [(I) and (M)] and 5 μm (K). Quantitative analysis of EdU (J)–, pH3 (L)–, and Aurora B (N)–positive cardiomyocytes at P70 mice hearts, $n = 5$. Data are presented as means ± SEM. By Student's t test, $^{*}P < 0.05$ and $^{***}P < 0.001$.

posterior wall thickness [LVPW;s (millimeters)], along with a dilation of the cardiac chamber internal diameter [LVID;s (millimeters)] (Fig. 3, Q to T, and table S1). Together, these findings indicate that *Ptma* is necessary for sustaining cardiomyocyte proliferation and neonatal heart regeneration in mice.

PTMA overexpression extends heart regenerative window

To explore whether PTMA is sufficient to promote heart regeneration, we infected P1 mice with AAV9-*Ptma* and performed MI at P8 (Fig. 4A). Immunostaining showed the overexpression of PTMA protein in cardiomyocyte nuclei (Fig. 4B). Compared with AAV9-*Luc*–infected control hearts, PTMA overexpression significantly increased the number of cardiomyocytes undergoing DNA synthesis and mitosis, as evidenced by EdU incorporation and pH3 staining (Fig. 4, C to G). We further observed a significantly higher proportion of Aurora B^{+} cardiomyocytes (Fig. 4, H and I). WGA staining of PTMA overexpression hearts showed a reduction in cardiomyocyte size (Fig. 4, J and K). These results demonstrate that PTMA overexpression effectively promotes the cardiomyocyte cell cycle reentry during the postnatal period post–MI injury.

Serial echocardiography was performed to determine whether cardiomyocyte proliferation induced by PTMA overexpression could contribute to the consequential cardiac repair following MI. The results revealed that PTMA overexpression significantly improved cardiac function, while, in AAV9-*Luc*–infected hearts, a progressive deterioration in cardiac function was observed following MI (Fig. 4, L to P, and data S1). Sirius red and Fast green co-staining showed that PTMA overexpression substantially reduced the size of the infarcted

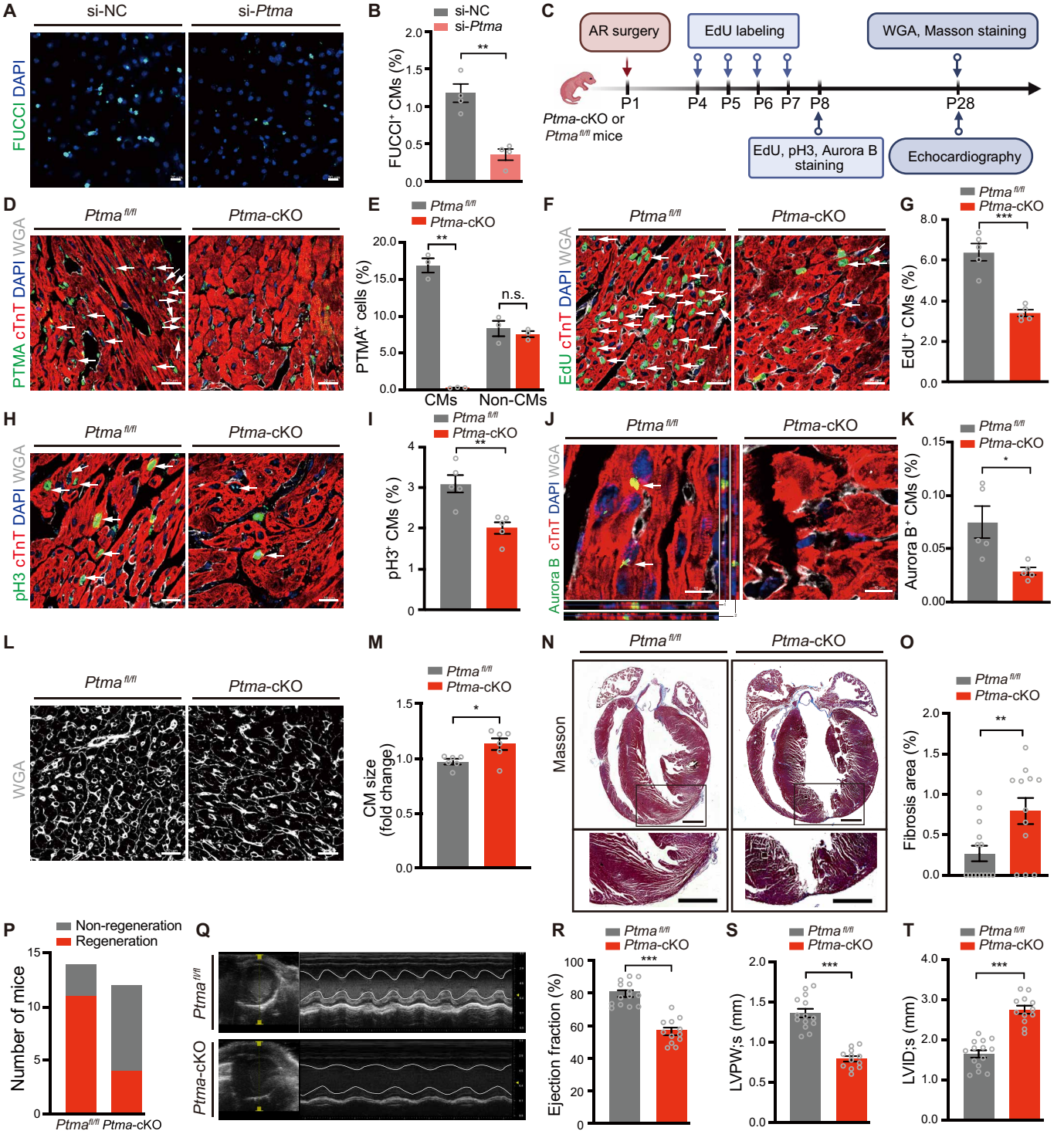

Fig. 3. *Ptma* is required for cardiomyocyte proliferation and heart regeneration. (**A** and **B**) Representative images (A) and quantitation of FUCCI$^+$ cardiomyocytes (B), $n = 4$. Scale bars, 20 μm. (**C**) Schematic showing the experimental procedure in *Ptma*-cKO mice, created in BioRender (S. Gai, 2025), https://BioRender.com/q64z784. (**D** and **E**) Immunostaining for PTMA (green) and cTnT (red) post-AR. Scale bars, 20 μm (D). Quantitation of PTMA-positive cells in cardiomyocytes and non-cardiomyocytes, $n = 3$ (E). (**F** to **K**) Representative immunostaining images for EdU (F), pH3 (H) and Aurora B (J). Scale bars, 20 μm [(F) and (H)] and 10 μm (J). Quantitation of EdU (G)–, pH3 (I)–, and Aurora B (K)–positive cardiomyocytes at 7 dpr, $n = 5$. (**L** and **M**) Wheat germ agglutinin (WGA) staining. Scale bars, 20 μm (L). Quantification of cardiomyocyte size in hearts at 7 dpr, $n = 6$ (M). (**N** to **P**) Representative images of Masson's trichrome staining. Scale bars, 1 mm (N). Quantification of the fibrosis area (O), and the number of regeneration or non-regeneration hearts at 28 dpr (P), $n = 14$ for *Ptma*$^{fl/fl}$ and $n = 12$ for *Ptma*-cKO group. (**Q**) M-mode echocardiography of the hearts at 28 dpr. (**R** to **T**) Echocardiography analyses of cardiac function of EF% (R), LVPW;s (S), and LVID;s (T) at 28 dpr, $n = 14$ for *Ptma*$^{fl/fl}$ and $n = 12$ for *Ptma*-cKO group. Data are means ± SEM. By Student's *t* test [(B), (E), (G), (I), (M), and (O)] and by Mann-Whitney test (K), $^*P < 0.05$, $^{**}P < 0.01$, and $^{***}P < 0.001$.

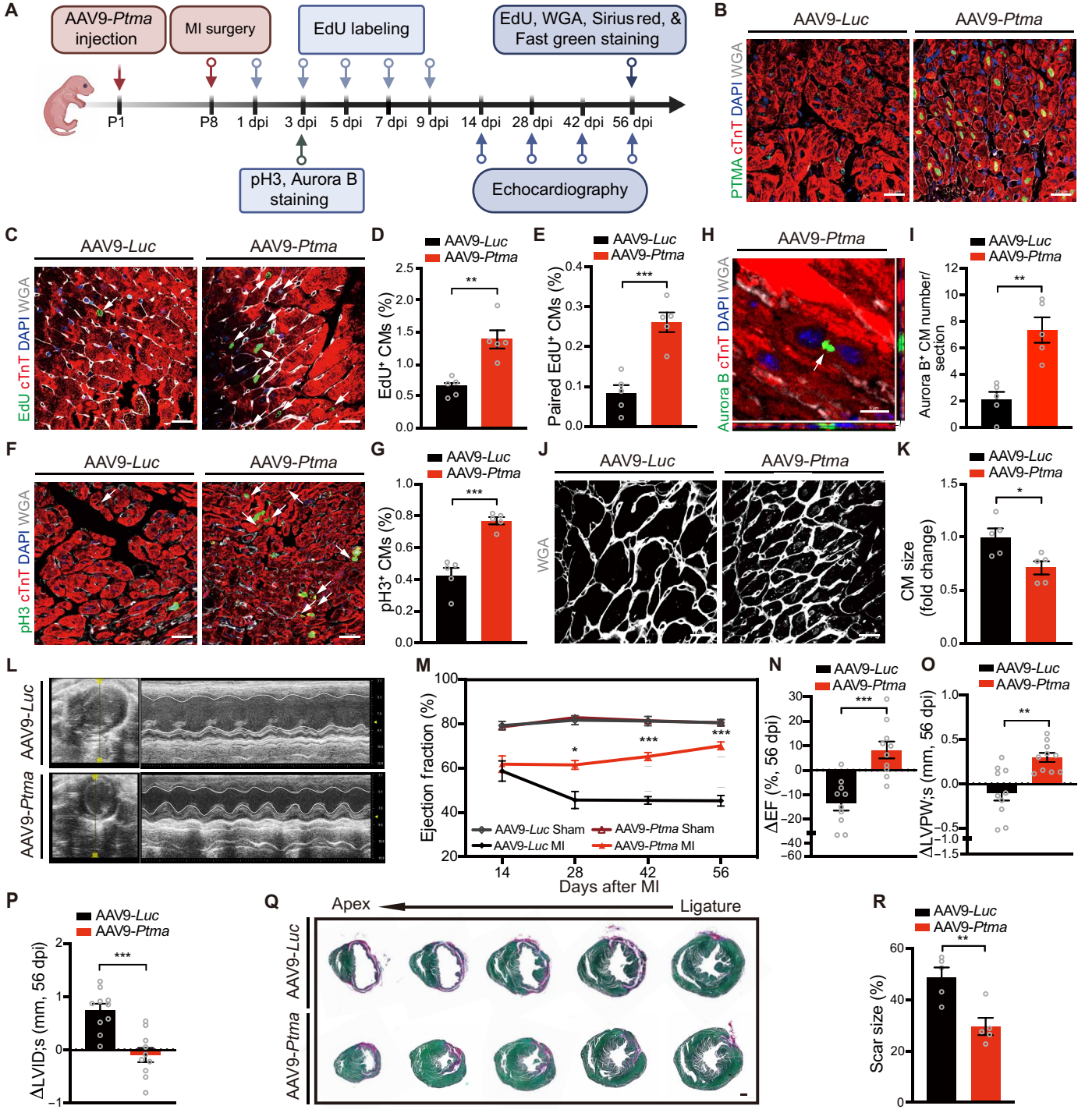

Fig. 4. PTMA overexpression extends heart regenerative window following MI injury. (**A**) Schematic plot showing the experimental procedure for AAV9-delivered PTMA overexpression following MI injury at P8, created in BioRender (S. Gai, 2025), https://BioRender.com/c86w605. (**B**) Representative images of PTMA (green) and cTnT (red) co-staining. Scale bars, 20 μm. (**C** to **I**) Representative immunostaining images for EdU (C), pH3 (F), and Aurora B (H) heart sections. Scale bars, 20 μm [(C) and (F)] and 10 μm (H). Quantitative analysis of EdU (D)–, adjacent EdU (E)–, pH3 (G)–, and Aurora B (I)–positive cardiomyocytes in hearts at 3 dpi. (**J** and **K**) WGA staining. Scale bars, 20 μm (J). Quantification of cardiomyocyte size at 56 dpi, $n = 5$ (K). (**L**) Representative images of M-mode echocardiography of mice at 56 dpi. (**M**) Echocardiography analyses of EF% in mice hearts from 14 to 56 dpi, $n = 6$ (sham) and $n = 10$ (MI). (**N** to **P**) Echocardiography analyses showing the change in EF% (N), LVPW;s (O), and LVID;s (P) in mice hearts at 56 dpi relative to 3 dpi, $n = 10$. (**Q** and **R**) Representative images of Sirius red/Fast green staining. Scale bar, 1 mm (Q). Quantification of the scar size (R) in hearts at 56 dpi. Sirius red/Fast green staining marks myocardium (green) and fibrosis scar (red), $n = 5$. Data are presented as means ± SEM. By Student's *t* test [(D), (E), (I), (K), (N), (O), (P), and (R)], by Mann-Whitney test (G), and by two-way ANOVA analysis (M), $^*P < 0.05$, $^{**}P < 0.01$, and $^{***}P < 0.001$.

area (Fig. 4, Q and R). These findings suggest that PTMA extends the heart regenerative window following MI injury.

PTMA augments adult cardiac regeneration and repair

To assess the potential of PTMA as a therapeutic target for treating adult MI, we induced MI in adult mice and delivered AAV9-*Ptma* via intramyocardial injection (Fig. 5A). Immunostaining showed the overexpression of PTMA protein in the infected hearts (Fig. 5B). We observed that PTMA overexpression improved heart morphology at 56 days postinfarction (dpi) compared to hearts infected with AAV9-*Luc* (Fig. 5C). Survival analysis revealed that PTMA overexpression significantly enhanced the survival rate following MI in adult mice, with a mortality rate of 14.3%, whereas the AAV9-*Luc* group exhibited a mortality rate of 40% at 14 dpi (Fig. 5D).

Serial echocardiography revealed that overexpression of PTMA significantly improved cardiac EF over time, whereas a progressive deterioration in cardiac function was observed in AAV9-*Luc*–infected hearts post-MI (Fig. 5, E to G; fig. S4A; and data S2). Consistent with this, AAV9-*Ptma*–infected hearts maintained LVPW;s (Fig. 5H) while decreasing LVID;s (Fig. 5I). Sirius red and Fast green co-staining revealed that overexpression of PTMA substantially reduced the infarct size (Fig. 5, J and K), further indicating that PTMA improves cardiac function and alleviates pathological cardiac remodeling. In sham hearts, PTMA overexpression had no significant impact on cardiac function or fibrosis (fig. S4, B to D, and data S2).

We then investigated whether PTMA overexpression induces cardiomyocyte proliferation in adult MI hearts. We observed that PTMA overexpression led to a reduction in cardiomyocyte size (fig. S4, E and F) and a significant increase in DNA synthesis (Fig. 6, A and B), as well as in cardiomyocyte mitosis and cytokinesis (Fig. 6, C to F). Moreover, we isolated adult cardiomyocytes from hearts injected with AAV9-*Luc* and AAV9-*Ptma* after MI and quantified the number of cardiomyocytes. The PTMA overexpression hearts exhibited a significant elevation in the total number of cardiomyocytes (Fig. 6, G and H). This result further corroborated the role of PTMA in promoting adult cardiomyocyte proliferation in response to MI. Furthermore, using inducible multicolor *R26R-Confetti Myh6-MerCreMer* reporter mice (fig. S4G) (*23*, *24*), we traced the de novo generation of cardiomyocytes and observed a significant increase in adjacent red fluorescent protein (RFP)–labeled and nGFP-labeled daughter cardiomyocytes in AAV9-*Ptma*–infected hearts compared to AAV9-*Luc*–infected hearts (Fig. 6, I to L). Together, these findings suggest that PTMA contributes

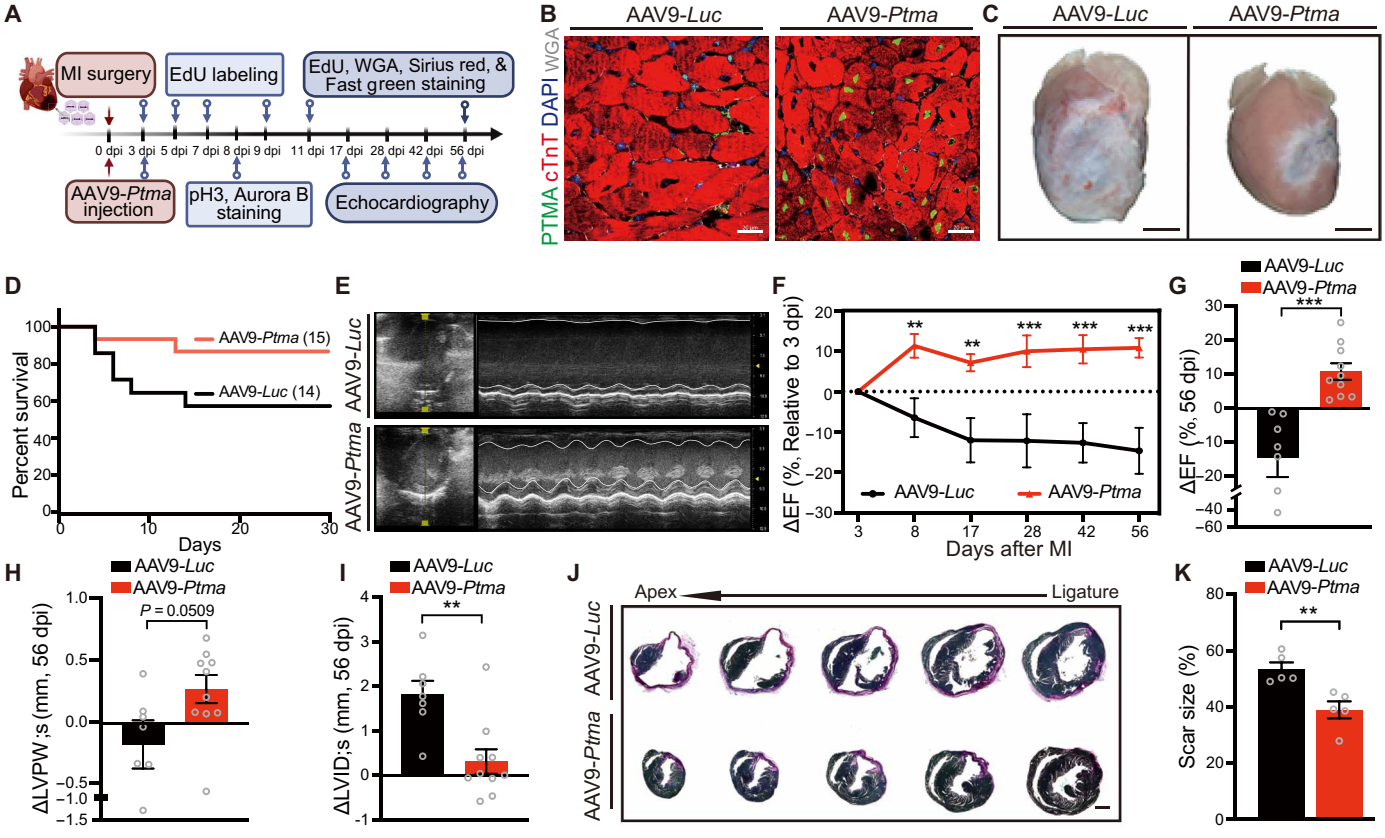

Fig. 5. AAV9-delivered *Ptma* gene therapy augments adult cardiac repair. (**A**) Schematic diagram showing the experimental procedure of AAV9-delivered therapeutic potential in adult MI injury, created in BioRender (S. Gai, 2025), https://BioRender.com/q64z784. (**B**) Representative images of heart sections stained with PTMA (green) and cTnT (red). Scale bars, 20 μm. (**C**) Representative images of heart morphology from AAV9-*Luc*– and AAV9-*Ptma*–treated hearts. Scale bars, 2 mm. (**D**) Survival curves of AAV9-*Ptma* group compared to AAV9-*Luc* group after MI injury, $n = 14$ (AAV9-*Luc*) and $n = 15$ (AAV9-*Ptma*). (**E**) Representative images of M-mode echocardiography of mice at 56 dpi. (**F**) Analyses of changes in EF from 3 to 56 dpi, $n = 7$ (AAV9-*Luc)* and $n = 10$ (AAV9-*Ptma*). (**G** to **I**) Bar chart with individual data points showing changes in EF% (G), LVPW;s (H), and LVID;s (I) at 56 dpi relative to 3 dpi, $n = 7$ (AAV9-*Luc*) and $n = 10$ (AAV9-*Ptma*). (**J** and **K**) Representative images of Sirius red/Fast green staining of series of transverse sections after MI injury, myocardium (green), and myocardial fibrosis scar (red). Scale bar, 1 mm (J). Quantification of scar size, $n = 5$ (K). Data are means ± SEM. By Student's *t* test [(B), (E), (G), (I), (M), and (O)] and by Mann-Whitney test (K), $^{**}P < 0.01$, and $^{***}P < 0.001$.

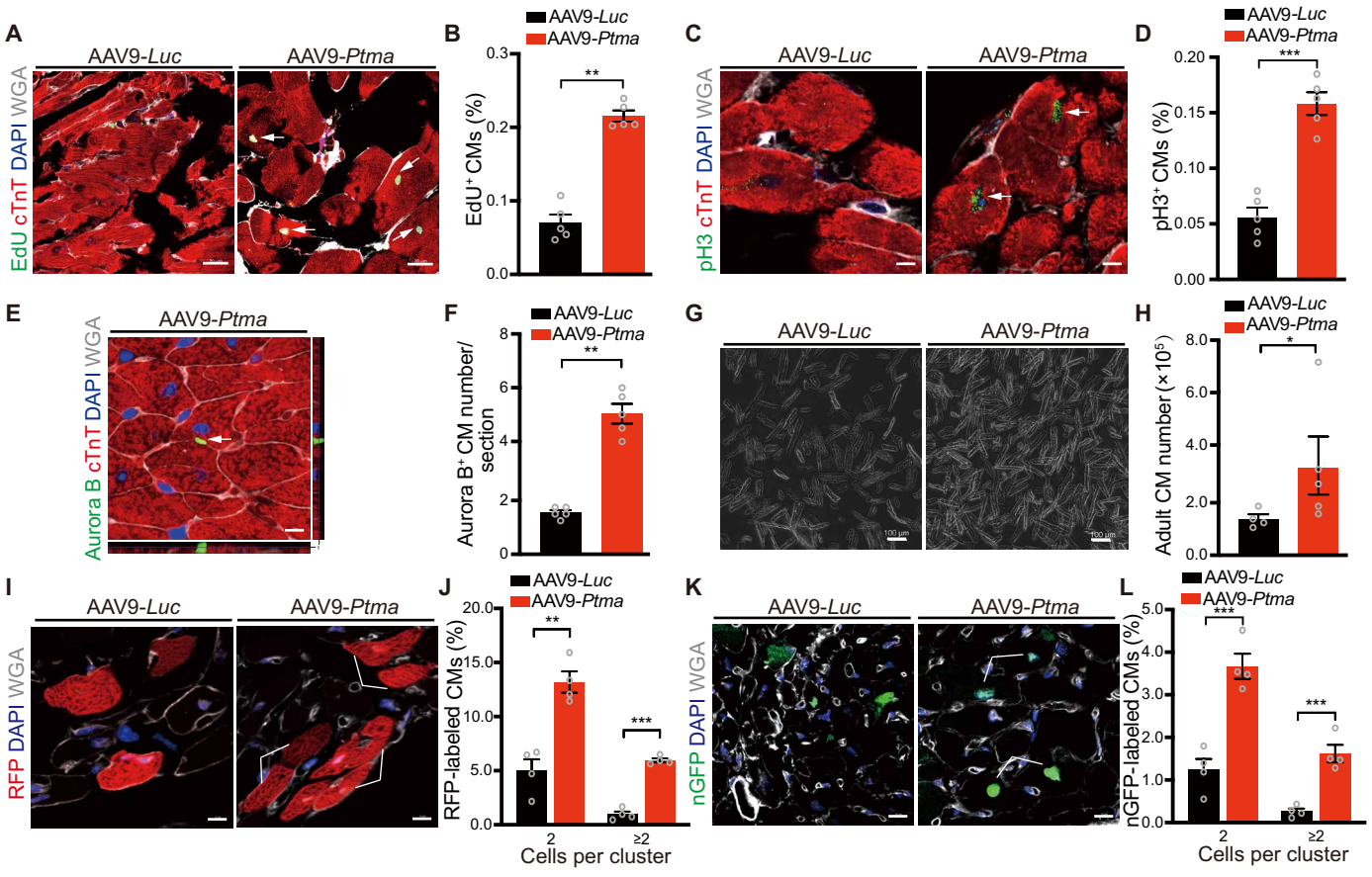

Fig. 6. AAV9-delivered *Ptma* gene therapy augments adult cardiac regeneration. (**A** to **F**) Representative images of immunostaining for EdU (A), pH3 (C), and Aurora B (E). Scale bars, 20 μm (A) and 5 μm [(C) and (E)]. Quantitative analysis of EdU (B)–, pH3 (D)–, and Aurora B (F)–positive cardiomyocytes in adult hearts at 7 dpi, $n = 5$. (**G** to **H**) Representative images of isolated adult cardiomyocytes. Scale bars, 100 μm (G). Quantification of the total number of cardiomyocytes at 2 weeks post–MI injury, $n = 4$ (AAV9-*Luc*) and $n = 5$ (AAV9-*Ptma*) (H). (**I** to **L**) Representative images of RFP$^+$ (I) and nGFP$^+$ cardiomyocytes (K). Scale bars, 5 μm (I) and 10 μm (K). Quantification of the clusters of two or more RFP$^+$ cardiomyocyte clones expansion (J) and nGFP$^+$ cardiomyocyte clones expansion (L) 2 weeks post-MI, $n = 4$. Data are presented as means ± SEM. By Student's *t* test, $^*P < 0.05$, $^{**}P < 0.01$, and $^{***}P < 0.001$.

to enhanced cardiac repair by promoting cardiomyocyte proliferation in adult hearts.

PTMA promotes hiPSC-CM proliferation

To explore the translational potential of PTMA, we overexpressed the human *PTMA* gene in human-induced pluripotent stem cell–derived cardiomyocytes (hiPSC-CMs) using an adenovirus delivery system (Ad-*PTMA*) (Fig. 7A). Western blot analysis showed the increased expression of human PTMA in hiPSC-CMs (Fig. 7B). EdU incorporation assays showed that PTMA overexpression increased the proportion of EdU$^+$ hiPSC-CMs to 6%, compared with 1.5% in cells infected with Ad-*Luc* (Fig. 7, C and D). Immunostaining demonstrated significant increases in both pH3$^+$ and Aurora B$^+$ hiPSC-CMs when PTMA was overexpressed (Fig. 7, E to H). Unbiased RNA-seq analysis of transcriptomes in hiPSC-CMs treated with Ad-*PTMA* revealed significant up-regulation of genes related to cell proliferation and development compared to Ad-*Luc* group, while genes involved in oxidative phosphorylation and apoptotic signaling pathways were down-regulated (Fig. 7, I to K). These results suggest that PTMA acts as a human cardiomyocyte proliferative factor, holding the potential for promoting human cardiac repair.

PTMA facilitates cardiomyocyte proliferation by inhibiting the deacetylation activity of MBD3/HDAC1 NuRD complex

PTMA is an unstructured, intrinsically disordered acidic nuclear protein which exerts its function mainly by binding to target proteins. To explore the interacting targets mediating PTMA-induced cardiomyocyte proliferation, we performed co-immunoprecipitation (co-IP) of MYC-tagged PTMA in cardiomyocytes using an adenovirus to deliver the MYC-tagged PTMA construct, and then we used mass spectrometry to identify PTMA-interacting proteins (Fig. 8A and fig. S5A). Because PTMA is a nuclear protein (Figs. 4B and 5B), we focused on the binding proteins mainly located in nucleus. A total of 25 nuclear proteins were identified (unique peptide ≥ 2, intensity ratio > 3, and score > 20) (Fig. 8B and table S2). To examine whether PTMA modulated cardiomyocyte proliferation through interaction with these targets, we knocked down the top four enriched PTMA binding proteins NSUN2, GRWD1, H2A/z, and MBD3 in PTMA-overexpressed cardiomyocytes using siRNA. Immunostaining of pH3 revealed the knockdown of *Mbd3* further enhanced PTMA-promoted proliferation of cardiomyocytes, while knockdown of *Nsun2*, *Grwd1*, and *H2az* had no significant effect (Fig. 8, C and D, and fig. S5, B and C). We further verified the interaction of PTMA with MBD3 by co-IP

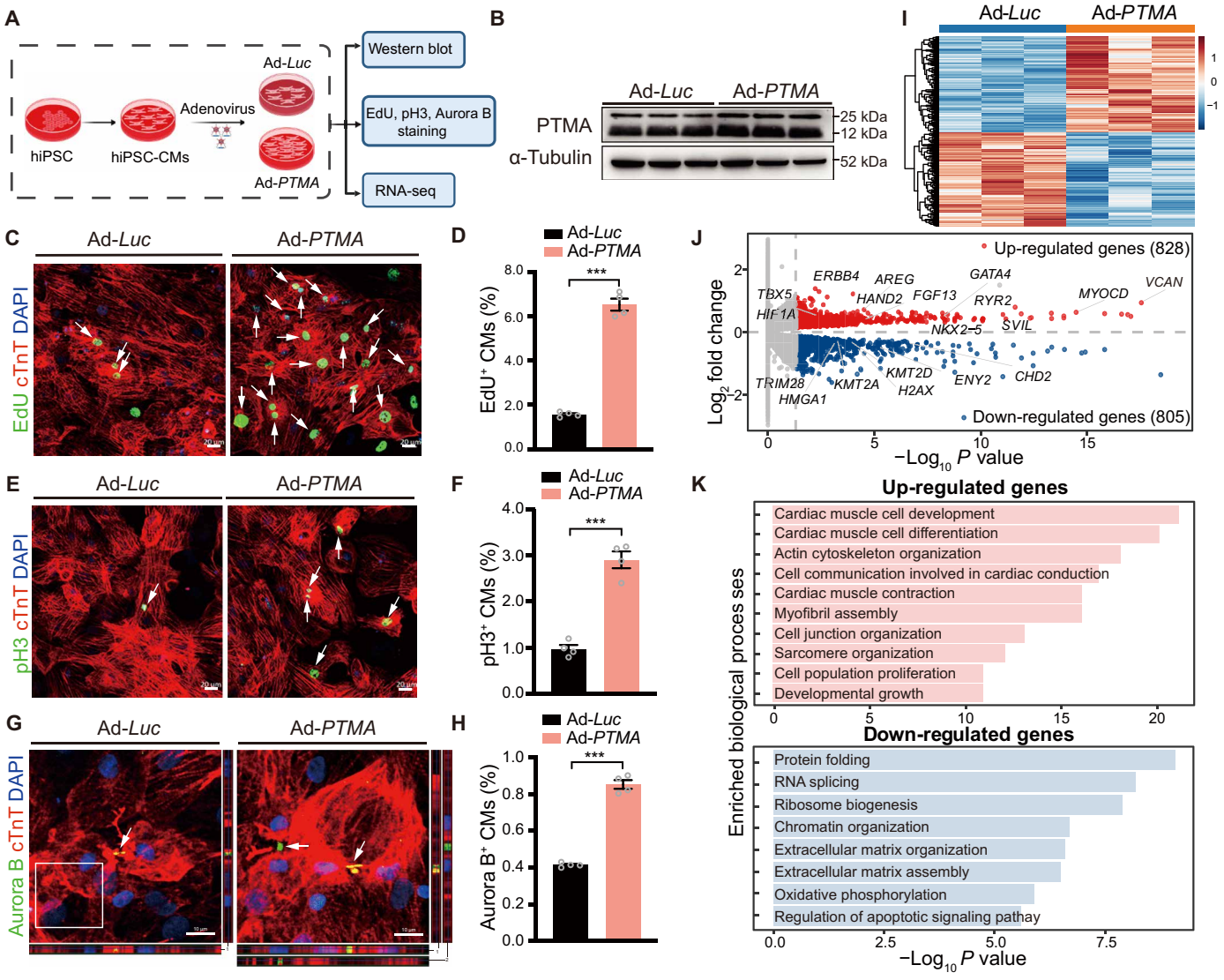

Fig. 7. PTMA promotes hiPSC-CM proliferation. (**A**) Schematic diagram showing the experimental procedure for Ad-*PTMA* treatment in hiPSC-CMs, created in BioRender (S. Gai, 2025), https://BioRender.com/c82t417. (**B**) Western blot of PTMA protein expression in hiPSC-CMs. (**C** to **H**) Representative images of EdU incorporation (C)–, pH3 (E)–, and Aurora B (G)–positive hiPSC-CMs treated with Ad-*PTMA* or Ad-*Luc*. Quantification of EdU (D)–, pH3 (F)–, and Aurora B (H)–positive hiPSC-CMs. Scale bars, 20 μm [(C) and (E)] and 10 μm (G), $n = 4$. (**I**) Hierarchical clustering of differentially expressed genes in Ad-*PTMA* versus Ad-*Luc* hiPSC-CMs as assessed by RNA-seq (adjusted P value < 0.05). (**J**) Volcano plot of 828 up-regulated and 805 down-regulated genes in Ad-*PTMA* versus Ad-*Luc* hiPSC-CMs, $n = 3$ in each group. (**K**) GO analysis of 828 up-regulated genes and 805 down-regulated genes in Ad-*PTMA* versus Ad-*Luc* hiPSC-CMs. Data are presented as means ± SEM. By Mann-Whitney test (D) and by Student's t test [(F) and (H)], ***$P < 0.001$.

(Fig. 8, E and F) and validated that PTMA co-localizes with MBD3 in cardiomyocytes by immunofluorescence staining (Fig. 8G). We further performed MBD3 IP on isolated WT neonatal cardiomyocytes and quantified the enrichment of its binding protein PTMA by normalizing to immunoglobulin G. The enriched PTMA in MBD3 IP further showed the endogenous interaction of PTMA with MBD3 (Fig. 8, H and I). We then knocked down *Mbd3* in cardiomyocytes and found that partial deletion of *Mbd3* leads to a significant increase in the proliferation of cardiomyocytes (Fig. 8, J and K). These data indicate that MBD3 mediates the role of PTMA in promoting cardiomyocyte proliferation.

MBD3 is an essential component of the NuRD complex, which comprises MBD3, HDAC1, CHD4, and other components (Fig. 8L) (*25*, *26*). The NuRD complex exhibits dual enzymatic functions: histone deacetylation via its HDAC proteins and chromatin remodeling via the adenosine triphosphatase (ATPase) CHD domain CHD4. Subsequently, we investigated whether the interaction between PTMA and MBD3 affects the function of the NuRD complex. We used MBD3 IP to assess the impact on NuRD complex interaction upon PTMA overexpression. The result demonstrated a significant reduction in MBD3's interaction with HDAC1, while the interaction between MBD3 and CHD4 remained unaffected (Fig. 8, M and N, and fig. S5D), indicating that overexpression of PTMA inhibits the deacetylation activity of MBD3/HDAC1 NuRD complex by disrupting the interaction between MBD3 and HDAC1.

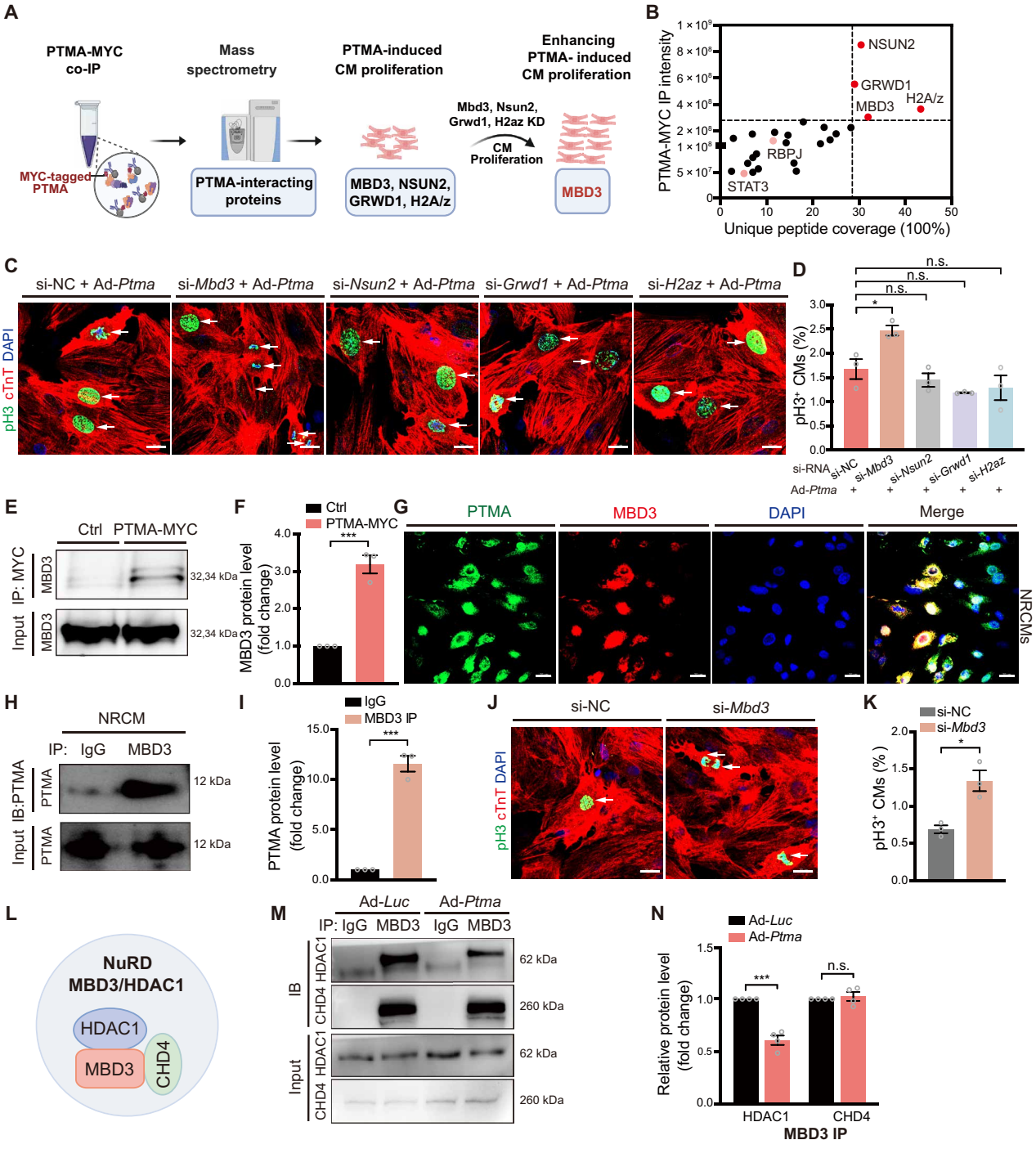

Fig. 8. PTMA facilitates cardiomyocyte proliferation by inhibiting the deacetylation activity of MBD3/HDAC1 NuRD complex. (**A**) Schematic showing the experimental procedure for identifying PTMA interacting proteins, created in BioRender (S. Gai, 2025), https://BioRender.com/j37x945. KD, knockdown. (**B**) The distribution of proteins identified from cardiomyocytes using Myc-tagged PTMA co-IP coupled mass spectrometry. (**C**) Representative immunostaining images for pH3. Scale bars, 20 μm. (**D**) Quantitative analyses of $pH3^+$ cardiomyocytes, $n = 3$. (**E** and **F**) Western blot of MBD3 protein expression in tagged MYC antibody immunoprecipitation (IP) in cardiomyocytes (E). Quantification of MBD3 protein enrichment that normalized to control (Ctrl) group (F), $n = 3$ independent replicates. (**G**) Immunostaining of PTMA, MBD3, and DAPI in cardiomyocyte nuclei. Scale bars, 20 μm. (**H** and **I**) Western blot of PTMA protein expression in MBD3 antibody IP in neonatal cardiomyocytes (H) and the quantification of PTMA protein enrichment that normalized to immunoglobulin G (IgG), $n = 3$ independent replicates (I). (**J** and **K**) Representative images of immunostaining for pH3 in NRCMs. Scale bars, 20 μm (J). Quantitative analyses of pH3-positive cardiomyocytes, $n = 3$ replicates (K). (**L**) Schematic of MBD3/HDAC1 NuRD complex. (**M** and **N**) Western blot of HDAC1 and CHD4 in MBD3 antibody IP in hypoxia cardiomyocyte lysate [3% O_2, (M)], immunoblot (IB). Quantification of HDAC1 and CHD4 enrichment in MBD3 IP, $n = 4$ independent replicates (N). Data are presented as means ± SEM. By one-way ANOVA analysis (D) and by Student's *t* test [(F), (I), (K), and (N)], $^*P < 0.05$ and $^{***}P < 0.001$; n.s. indicates the *P* value is not statistically significant.

PTMA promotes cardiomyocyte proliferation by acetylating STAT3

To explore how PTMA represses the deacetylation function of the MBD3/HDAC1 NuRD complex, we investigated the interacting nuclear proteins in PTMA co-IP. Among them, only STAT3 and RBPJ are reported to undergo direct deacetylation by HDAC1 (Fig. 8B and table S2). STAT3 is a pleiotropic transcription factor, which plays an important role in regulating genes involved in cell proliferation and survival (*27*). Acetylation at Lys^{685} was crucial for STAT3 to form stable dimers, which may potentially prevent phosphatases from binding to STAT3, thereby maintaining higher phosphorylation levels, which enabled STAT3 to enhance the transcription of cell growth related genes and promote cell cycle progression (*28*, *29*). Deacetylation of STAT3 by HDACs can shut down its activity (*29*). Previous research from our laboratory and others has established STAT3 phosphorylation activation as a regenerative therapeutic strategy for MI (*30*, *31*). RBPJ is a major downstream effector of the Notch signaling pathway (*32*). As PTMA overexpression post-MI promotes the phosphorylation activation of STAT3 without affecting the expression of NICD, which reflects the Notch signaling pathway activation (Fig. 9, A and B), we mainly focused on PTMA's regulation of STAT3. Our MYC-tagged PTMA co-IP identified an interaction between PTMA and STAT3 in cardiomyocytes (Fig. 9, C and D). We then performed STAT3 IP, which showed that PTMA treatment reduced the interaction between STAT3 and HDAC1, leading to elevated lysine acetylation of STAT3 (Fig. 9, E and F). The Western blot further showed that there was boosted STAT3 acetylation and phosphorylation upon PTMA overexpression in hypoxic neonatal rat cardiomyocytes (NRCMs) (Fig. 9, G and H). In contrast, knockdown of *Ptma* in cardiomyocytes inhibited STAT3 acetylation and phosphorylation (Fig. 9, I and J). To further reveal that PTMA promotes STAT3 acetylation and phosphorylation activation by blocking the deacetylation activity of the MBD3/HDAC1 NuRD complex, we knocked down *Mbd3* to disrupt the function of the NuRD complex and found that *Mbd3* knockdown boosted acetylation and phosphorylation of STAT3 (Fig. 9, K and L) and promoted the transcriptional activation of STAT3-targeted genes (Fig. 9M), including *Myc*, *Pim1*, *Birc5*, and *Cryab*, which have been reported to regulate cardiomyocyte proliferation and survival (*33*–*36*).

Last, we tested whether PTMA promoted cardiomyocyte proliferation by activating STAT3. We knocked down *Stat3* in PTMA-overexpressing cardiomyocytes and found that *Stat3* repression almost completely abrogated the proliferative effect induced by PTMA (Fig. 9, N and O, and fig. S6, A and B). These results indicate that PTMA enhances cardiomyocyte proliferation mainly by blocking the deacetylation function of the MBD3/HDAC1 NuRD complex, which, in turn, leads to the elevated STAT3 acetylation and activation of the genes involved in cell proliferation and survival (Fig. 10).

DISCUSSION

The limited regenerative capacity of the adult mammalian heart significantly hinders recovery and survival following MI (*2*, *4*). In contrast, the fetal and neonatal hearts exhibit robust regenerative capabilities due to their retention of the fetal gene program (*7*, *8*). Understanding the fetal gene program in hearts with different regenerative abilities is crucial for identifying previously unknown therapeutic targets to enhance cardiac repair. In this study, we conducted scRNA-seq of embryonic hearts and identified *Ptma* as a key regulator of embryonic cardiomyocyte proliferation. The deletion of *Ptma* suppresses cardiomyocyte proliferation and neonatal heart regeneration. Conversely, cardiomyocyte-specific overexpression of PTMA extends the proliferative time window of cardiomyocytes. We observed that PTMA overexpression enhances cardiac repair by promoting cardiomyocyte proliferation in neonatal and adult hearts, suggesting that PTMA is an effective therapeutic target for heart regeneration. Furthermore, PTMA induces the proliferation of hiPSC-CMs, highlighting its potential for promoting human cardiac repair. Mechanistically, we demonstrated that PTMA interacted with MBD3, thereby competitively inhibiting the deacetylation activity of MBD3/HDAC1 NuRD complex. This inhibition leads to increased acetylation of STAT3, enhancing its phosphorylation and activation of genes involved in cell proliferation and survival.

During early heart development, clonal expansion of proliferating cardiomyocytes is responsible for embryonic heart growth and normal morphogenesis. The events of coherent proliferation and clonal expansion of cardiomyocytes were found as early as E8.5 when heart tube looping initiated and started to decrease around E12.5 (*37*). We collected embryonic hearts at seven developmental time points (E8.5, E9.0, E9.5, E10.5, E11.5, E14.5, and E17.5) and conducted scRNA-seq. These scRNA-seq data provide a source of information for research into embryonic heart development and cardiomyocyte proliferation. We defined the proliferative cardiomyocyte population on the basis of the cell cycle scoring analysis and the expression of cell cycle marker genes *Mki67* and *Aurkb* in the scRNA-seq data. Our results showed that, among the 17964 cardiomyocytes, 18.78% were proliferative, while 81.22% had exited the cell cycle during embryonic development. Through comparative analysis of these two populations, we identified 120 genes significantly enriched in proliferative cardiomyocytes. As cardiomyocytes rapidly arrest their cell cycle within the first postnatal week, we introduced our bulk RNA-seq data from purified cardiomyocytes during postnatal heart development. This includes data from regenerative stages (E14.5, P1, and P4) and non-regenerative stages (P7, P14, and P56) (*19*). Consequently, we identified three key genes—*Ptma*, *Tubb5*, and *Tuba1b*—that were highly expressed in embryonic proliferative cardiomyocytes and decreased during heart development. Subsequent functional experiments revealed that PTMA enhances cardiomyocyte proliferation effectively, indicating that PTMA is a potential target for heart regeneration.

PTMA is essential for embryonic development, and homozygous *Ptma* knockout mice exhibit lethality at an early embryonic stage (*38*). Furthermore, a reduction in PTMA level in embryos leads to cell apoptosis and defects in cell proliferation (*39*). In contrast to a previous report that the combination of PTMA and TMSB4 acts as a promoter of cardiac regeneration (*40*), our study found that *Ptma* is enriched in embryonic proliferating cardiomyocytes, and that *Ptma* deficiency suppresses cardiomyocyte proliferation and neonatal heart regeneration. We also revealed that AAV9-mediated PTMA overexpression promotes adult heart regeneration post–MI injury, as evidenced by increased cardiomyocyte proliferation and clonal expansion, reduced scar area, and improved heart function. Furthermore, the conserved proliferative effect of PTMA on hiPSC-CMs underscores its potential for clinical application. The transiently elevated serum levels of PTMA in patients early after myocardial ischemia-reperfusion are associated with better prognosis (*41*). Collectively, these findings underscore PTMA as a therapeutic target for cardiac regenerative repair.

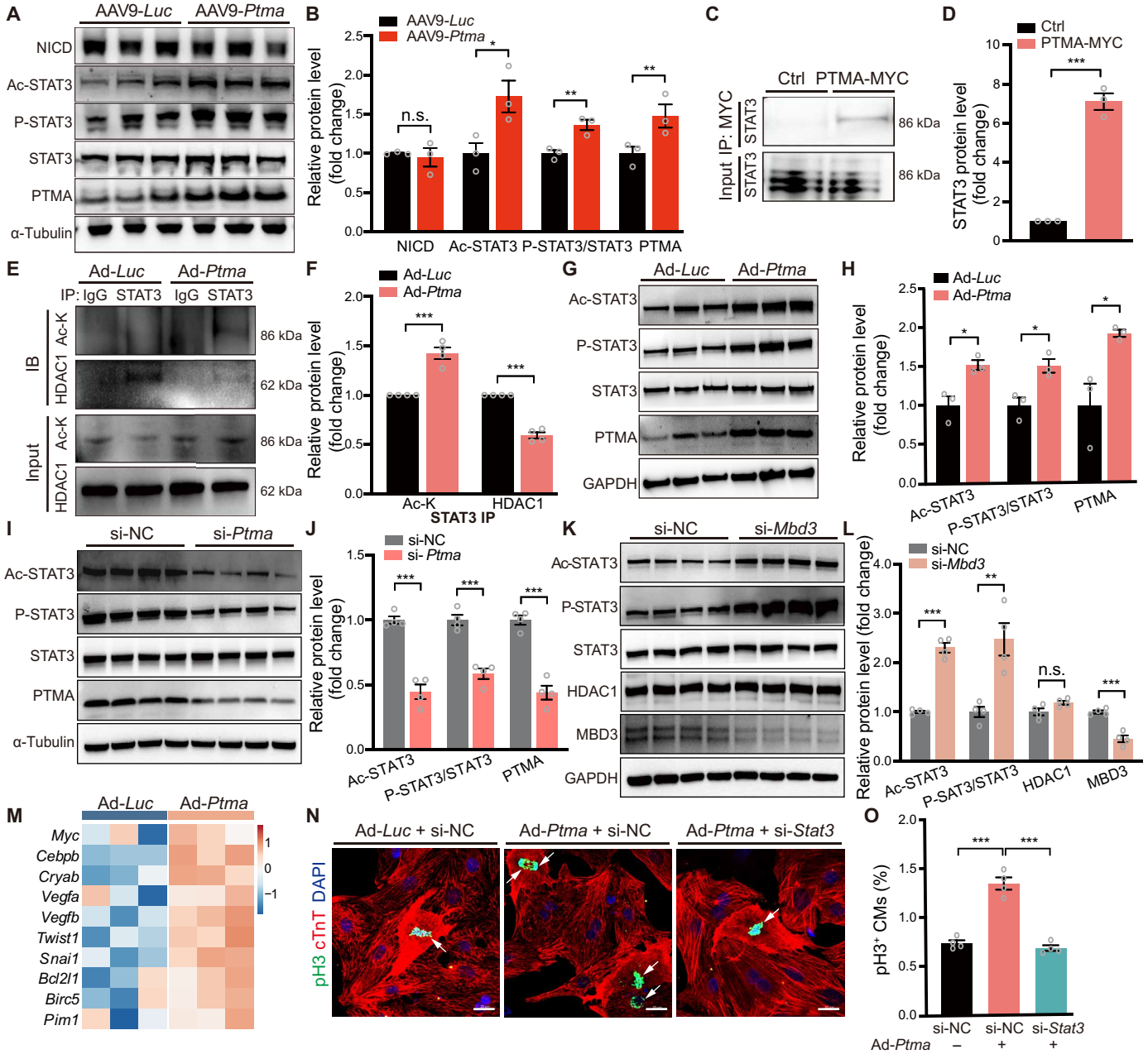

Fig. 9. PTMA promotes cardiomyocyte proliferation by acetylating STAT3. (**A** and **B**) Western blot of Notch and STAT3 signaling pathway post-MI (A), and quantification of the protein expression, $n = 3$ (B). (**C** and **D**) Western blot of STAT3 protein expression in tagged MYC antibody IP in cardiomyocytes (C). Quantification of STAT3 protein enrichment that normalized to Ctrl group, $n = 3$ independent replicates (D). (**E** and **F**) Western blot of HDAC1 and acetylated lysine (Ac-K) in STAT3 antibody IP in hypoxia cardiomyocyte lysate [3% O_2, (E)]. Quantification of protein enrichment, $n = 4$ independent replicates (F). (**G** and **H**) Western blot of STAT3 signaling pathway in hypoxia cardiomyocyte lysate [3% O_2, (G)]. Quantification of the protein expression, $n = 3$ (H). (**I** and **J**) Western blot of STAT3 signaling pathway in hypoxia embryonic cardiomyocytes [3% O_2, (I)]. Quantification of the protein expression, $n = 4$ replicates (J). (**K** and **L**) Western blot of STAT3 signaling pathway in hypoxia cardiomyocyte lysate [3% O_2, (K)]. Quantification of the protein expression, $n = 4$ (L). GAPDH, glyceraldehyde-3-phosphate dehydrogenase. (**M**) Heatmap of STAT3 target gene expression in hypoxia cardiomyocyte (3% O_2). (**N** and **O**) Representative images of immunostaining for pH3 in NRCMs. Scale bars, 20 μm (N). Quantitative analyses of pH3-positive cardiomyocytes, $n = 4$ replicates (O). Data are presented as means ± SEM. By Student's *t* test [(B), (D), (F), (H), and (J)] and by one-way ANOVA analysis (O), $^*P < 0.05$, $^{**}P < 0.01$, and $^{***}P < 0.001$; n.s. indicates the *P* value is not statistically significant.

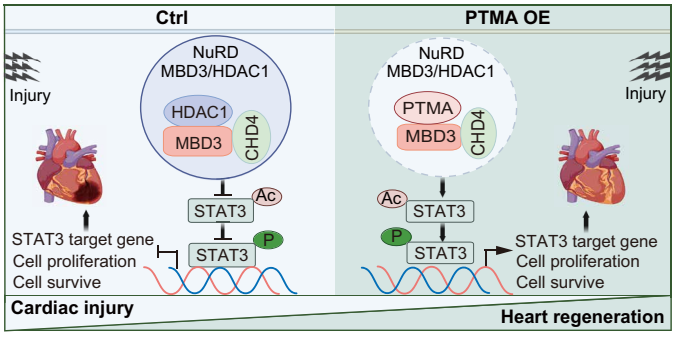

Fig. 10. Schematic showing the mechanism of PTMA-regulated cardiomyocyte proliferation and cardiac repair. Created in BioRender (S. Gai, 2025), https://BioRender.com/o67l028, with modification. PTMA interacts with MBD3, competitively inhibiting the deacetylation activity of MBD3/HDAC1 NuRD complex. This inhibition leads to increased acetylation of STAT3 and enhances STAT3 phosphorylation and the activation of genes related to cardiomyocyte proliferation and survival. Consequently, PTMA promotes cardiac regeneration and repair. OE, overexpression.

PTMA is an intrinsically disordered protein that functions through three identified mechanisms. First, it can be secreted from cardiomyocytes to stimulate angiogenesis (*42*). Second, it can translocate from the nucleus to the cytoplasm, where it protects cells from apoptosis (*14*). Third, within the nucleus, PTMA serves as a chromatin regulator, further contributing to its multifunctional capabilities (*15*, *16*, *43*, *44*). In our study, we found that PTMA is located in cardiomyocyte nuclei and promotes cardiomyocyte proliferation. We performed co-IP of MYC-tagged PTMA in cardiomyocytes to systematically identify proteins that interact with the nuclear PTMA. We uncovered an unrecognized PTMA-interacting protein MBD3, which is an essential structural protein required for the stable formation of the MBD3/NuRD complex (*25*, *45*). The NuRD complex exhibits dual enzymatic functionality, histone deacetylation through its HDAC proteins, and chromatin remodeling through its ATPase CHD domains (*46*, *47*). Knockdown of *Mbd3* leads to the disassembly of the MBD3/NuRD complex, preventing histone deacetylation and chromatin compaction (*25*, *26*, *45*). Furthermore, *Mbd3* deficiency is involved in the regulation of pluripotency and self-renewal of mouse embryonic stem cells (*26*, *48*). In this study, we elucidated the translational deacetylation modification of the MBD3/HDAC1 NuRD complex on STAT3. We further provided multiple lines of evidence supporting that PTMA promotes cardiomyocyte proliferation by inhibiting the deacetylation function of this complex. First, the MBD3 IP showed PTMA reduced the recruitment of deacetylase HDAC1 without affecting adenosine 5′-triphosphate–dependent chromatin remodeling enzyme CHD4 (Fig 8, M and N). Second, we observed that PTMA enhances STAT3 acetylation and phosphorylation activation by blocking the MBD3/HDAC1 NuRD complex's deacetylation activity (Fig 9, E and F). Third, the inhibition of *Stat3* in PTMA-overexpressing cardiomyocytes almost completely abrogated the proliferation induced by PTMA (Fig 9, N and O). These data indicate that PTMA enhances cardiomyocyte proliferation mainly by inhibiting the deacetylation activity of the MBD3/HDAC1 NuRD complex, thereby promoting STAT3 acetylation and phosphorylation activation. In this study, we revealed that both native PTMA and overexpressed PTMA regulate cardiomyocyte proliferation by increasing STAT3 acetylation and phosphorylation activation. We have established a strong correlation between PTMA-promoted cardiomyocyte proliferation and increased STAT3 acetylation and phosphorylation, which is achieved by disrupting the inhibitory effect of the MBD3/HDAC1 NuRD complex. Our group and other studies have shown that STAT3 activation effectively promotes cardiomyocyte proliferation and cardiac regeneration (*49*–*51*). STAT3 signaling regulates cardiomyocyte and other cell proliferation by initiating the transcription of cell cycle genes such as *c-Myc*, *Pim1*, *Cryab*, *Birc5*, *Ccnd1*, *Cdkn2b*, and *Cdkn1a* (*33*–*36*, *52*–*54*). We validated that PTMA overexpression increased the expression of most of these cell cycle genes, and the bioinformatics analysis revealed that those cell cycle genes, which are regulated by STAT3, are up-regulated in *Ptma* highly expressed VCM1 (fig. S6C). More studies still need to be done to validate the NuRD-HDAC1-STAT3 downstream targets. In addition, we could not exclude the possibility that other proteins may also be modified by the MBD3/HDAC1 NuRD complex, contributing to PTMA-promoted cardiomyocyte proliferation. However, the observation that *Stat3* inhibition in PTMA-overexpressing cardiomyocytes almost completely blocked PTMA-induced cardiomyocyte proliferation corroborates the critical role of STAT3 acetylation in this process.

Collectively, our study provides comprehensive scRNA-seq data across seven time points of embryonic heart development, mapping the dynamic expression of various cell types and offering a valuable resource for cardiac development research. On the basis of these data, we focused on analyzing the gene expression differences between proliferating and non-proliferating cardiomyocytes during embryonic development, identifying PTMA as a key regulator of the cardiomyocyte cell cycle. We discovered that PTMA, as a nuclear protein, binds to MBD3, thereby removing the suppressive effects of the MBD3/HDAC1 NuRD complex on STAT3 acetylation. By combining the results from MI animal intervention experiments and hiPSC-CMs studies, we demonstrate that targeting PTMA presents a promising therapeutic avenue for augmenting cardiomyocyte proliferation and fostering heart regeneration. These findings highlight potential previously unidentified intervention targets and strategies for patients suffering from ischemic heart disease.

MATERIALS AND METHODS

Animals

P1, P8, and adult mice were provided by Vital River Laboratory Animal Technology Co. Ltd. (Beijing, China). Neonatal mice were provided by SiPeiFu Biotechnology Co. Ltd. (Beijing, China). The *Myh6-Cre* (no. C00041) and *Ptma*$^{fl/fl}$ (S-CKO-04569) mice were constructed by Cyagen Bioscience (Suzhou, China), cardiomyocyte-specific *Ptma* knockout (*Ptma*-cKO) mice were generated by crossing *Ptma*$^{fl/fl}$ mice with Myh6-Cre strains, and *Ptma*$^{fl/fl}$ mice were used as controls. The *Myh6-MerCreMer* mice with a loxP-flanked multicolor fluorescent protein confetti mouse line (*23*, *24*) were supplied by J. Chen at the Institute of Translational Medicine, Zhejiang University (Hangzhou, China). All animal experiments were conducted in accordance with the Guide for the Use and Care of Laboratory Animals, and all animal protocols were approved by the Institutional Animal Care and Use Committee, Fuwai Hospital, Chinese Academy of Medical Sciences. The study approval number is FW-2021-0052.

AR operation

The neonatal *Ptma*-cKO and control mice at P1 underwent AR operation (*49*). In brief, the neonatal mice were anesthetized on ice for 2 min, and a transverse incision was made in the skin of the lower

half of the left breast using microscissors. The intercostal muscles were bluntly dissected to expose the inner chest cavity between the third and fourth intercostal spaces. After that, the heart was exteriorized by pressing on the abdomen to obtain a better operation field, and 15% of the apical tissue was resected immediately. The thoracic wall and skin incision were closed using 8-0 silk sutures. Mice were then placed on a heating plate at 37°C until recovery. The sham-operated mice underwent the same procedures as mentioned above without AR.

MI model

MI procedures were performed on P8 and adult mice (*55*, *56*). For P8 MI, the mice were anesthetized on ice for 3 min, after which the chest was opened to expose the heart without intubation. The left anterior descending coronary artery (LAD) was permanently ligated with 8-0 silk sutures. Subsequently, the dissected intercostal space and chest skin were sutured using 6-0 silk sutures (Ethicon, USA). For the sham group, the mice underwent the same procedure without LAD ligation. Last, the mice were allowed to recover on a heating plate at 37°C after the operation.

The adult MI model was performed on 2-month-old C57BL/6 mice by ligating the LAD. In detail, the adult mice were anesthetized with isoflurane, the chest was depilated and cleaned with 75% alcohol and, then, a suture was placed around the front upper incisors and pulled taut so that the neck was extended. A 20-gauge catheter was inserted into the trachea and connected to the mouse ventilator via a Y-shaped connector. For a 25-g mouse, the tidal volume was about 225 μl, and the respiratory rate was 110 breaths per minute. Then, the chest was opened through a left parasternal incision, the intercostal muscles between the third and fourth intercostal spaces were separated by blunt dissection until the inner chest cavity was exposed, a chest retractor was used to facilitate the view. The pericardium was opened, and the LAD was ligated with 7-0 silk sutures (Ethicon, USA). Subsequently, a 4-0 silk suture (Ethicon, USA) was used to suture the dissected intercostal space and chest skin. After the operation, the mice were allowed to recover on a heating plate at 37°C.

Genotyping of mice

For mouse genotyping, the DNA was extracted from mouse tail tissue using an alkaline lysis method, followed by neutralization with tris-HCl to halt the lysis. PCR amplification was performed using a 2× Taq Master Mix (Vazyme, P112-01), with the genotyping primers listed in Data S3. Subsequently, 3% agarose gel electrophoresis was performed to distinguish the WT and positive mutant bands.

Echocardiography

Echocardiography was conducted using Visual Sonics Vevo 2100 Imaging System (Visual Sonics, Toronto, Canada), along with an 18- to 38-MHz transducer (model MS-400/MS-550). MS-550 was used for 1-month-old mice and MS-400 for the adult mice. The dimensions of the left ventricle (LV), which include the diastolic and systolic wall thicknesses, as well as LV end-diastolic and end-systolic chamber dimensions, were measured using two-dimensional short-axis under M-mode tracings near the papillary muscle. Using these primary measurements, key functional parameters such as ejection fraction (EF%), fractional shortening (FS%), and left ventricular volume were accurately calculated. Additionally, the left ventricular (LV) dimensions, including diastolic (LVPW;d) and systolic (LVPW;s) wall thicknesses, and the left ventricular internal diameter at end-diastole (LVID;d) and end-systole (LVID;s) were determined as previously described (*21*).

Histology and immunostaining of heart sections

The mouse hearts were excised and fixed in 4% paraformaldehyde overnight (P8 MI hearts or 7-dpr hearts) or for 24 hours (adult hearts). After serial dehydration using an automatic tissue dehydrator (Leica, ASP300S, Germany), the heart tissues were processed and embedded in paraffin wax using standard laboratory procedures, and, then the paraffin blocks were sectioned from the infarct site to the apex at a thickness of 4 μm to determine infarct size. The first five sections of every 200 to 300 μm were selected for staining with Fast green/Sirius red using a modified Sirius Red stain kit (Solarbio, G1472) according to the user manual. ImageJ was used to quantify the fibrosis area. Infarct fibrosis was calculated following the formula: [length of coronal infarct perimeter (epicardial + endocardial)/total left ventricular coronal perimeter (epicardial + endocardial)] × 100 (*56*). The Masson's staining of the AR heart was performed using the Masson's Trichrome Stain Kit (Solarbio, G1340) according to the manufacturer's instructions. The fibrosis area of the heart was determined on the basis of Masson's staining result (*30*). Heart regeneration is a comprehensive metric established on the basis of significant activation of cardiomyocyte proliferation, minimal fibrotic scarring, and recovery of cardiac function.

The immunofluorescence staining was performed on paraffin-embedded heart sections to assess the proliferation and the areas of cardiomyocytes. All proliferation detections were conducted in the peri-infarct zones. After undergoing deparaffinization, rehydration, and heat-induced antigen retrieval, the heart sections were permeabilized with 0.5% Triton X-100 and blocked with 5% donkey serum for 1 hour at room temperature (RT). The primary antibody was incubated at 4°C overnight. Before incubation with the secondary antibody, the heart sections with the primary antibody were recovered at RT for 45 min, followed by washing three times with phosphate-buffered saline (PBS). Last, the heart sections were sealed with a mounting medium with 4′,6-diamidino-2-phenylindole. The Vectra Polaris automatic quantitative pathological imaging analysis system (PerkinElmer, USA) was used for scanning the immunofluorescence images of the whole-tissue section and quantifying cardiomyocyte proliferation. ImageJ software was used to measure the size of cardiomyocytes in the papillary muscles. The representative immunofluorescence images were all captured by a ZEISS LSM800 confocal laser scanning microscope (ZEISS, Germany). The sources of proliferation primary and secondary antibodies are listed in table S3.

Cell lines

hiPSC-CMs (CA2201106 hiPSC-CM cell line) were provided by Cellapy Biotechnology Co. Ltd. (Beijing, China). Cells were cryopreserved in liquid nitrogen until thawed and cultured according to the manufacturer's instructions. Coat Costar 6-well or 48-well cell plates with Matrigel (Corning, 354277) for 2 hours at 37°C. Then, the cryopreserved hiPSC-CMs were thawed and plated on Costar 6-well (60×10^4 cells per well) or 48-well cell plates (7.5×10^4 cells per well) and cultured with CardioEasy hiPSC-CM maintenance medium (Cellapy, CA2013100). The medium was replaced every 48 hours.

Mouse and rat primary cardiomyocyte isolation and culture

Mouse cardiomyocytes were isolated from E17.5/P1 WT mouse hearts, and the rat cardiomyocytes were isolated from P1 hearts by

using the Neonatal Heart Dissociation Kit in combination with gentleMACS and Octo Dissociator (Miltenyi BioTec, Teterow, Germany). The experiment was conducted according to the kit manufacturer's instructions. The dissociated cardiac cells were then subjected to a red blood cell lysis to remove erythrocytes. After that, the cardiac cells were seeded into Dulbecco's modified Eagle's medium (DMEM; Gibco, 11885) medium supplemented with 10% fetal bovine serum (FBS; Gibco, 10437077) in a 5% CO_2-humidified incubator at 37°C for 40 min to separate cardiomyocytes and non-myocytes. The suspension cardiomyocytes were used for downstream experiments.

Adult cardiomyocytes isolation and counting

Adult hearts were harvested at 2 weeks after MI. Then, immediately fixed in 4% paraformaldehyde (PFA) at RT for 1 to 2 hours. After fixation, the 4% PFA was aspirated and discarded. Using forceps, each heart was transferred to a new 5-ml EP tube and washed three times with sterile PBS. Subsequently, the hearts were cut into 3-mm pieces and incubated with collagenase B (1.8 mg/ml, Roche) and collagenase D (2.4 mg/ml, Roche) in sterile PBS supplemented with ampicillin (100 μg/ml, Beyotime) at 37°C on an end-over-end shaker. Every 24 hours, the enzyme solution containing dissociated cardiomyocytes was collected into a 15-ml centrifuge tube. Fresh enzyme solution was then added to the remaining heart tissue in the 5-ml EP tube. This process of collection and addition was repeated until no more cardiomyocytes could be dissociated from the tissue. The collected enzyme solutions were filtered through a 160-μm nylon mesh to obtain the supernatants. The filtered supernatants were pooled together. The cell suspension was gently pipetted to ensure uniform mixing. A 15-μl aliquot of the cell suspension was aspirated and transferred to a Countstar. A Keyence microscope was used to scan the Countstar for photography and perform cell counting (*56*–*58*).

Primary cell culture

All primary cells were cultured at 37°C in a 5% CO_2-humidified incubator (Thermo Fisher Scientific, Germany). For hypoxic culture, cardiomyocytes were cultured in a Heracell VIOS 160i CO_2 incubator at 37°C and 3% O_2 (Thermo Fisher Scientific, Germany) to induce hypoxia.

AAV9, adenovirus, and lentivirus

AAV9 and adenovirus were both provided by Vigene Bioscience Company (Jinan, China). AAV9-cTNT: *Ptma* (AAV9-*Ptma*) was generated in the AAV9 vector, using the cardiac-specific Tnnt2 promoter to facilitate the expression of *Ptma* specifically in cardiomyocytes (*21*). An AAV9-cTNT: Luciferase (AAV9-*Luc*) served as a control. Adenovirus-mediated *Ptma* gene overexpression was under the cytomegalovirus (CMV) promoter, and Ad-*Luc* was used as a control. PTMA, TUBB5, and TUBA1B were constructed as fusion proteins. These proteins were fused with an human influenza hemagglutinin (HA) tag on lentivirus vectors under the CMV promoter and were packaged into lentivirus by GenePharma (Suzhou, China). The null lentivirus vector was used as a control.

The pAdeno vector pAdeno-cTNT-MAG-hegenmin of the green FUCCI reporter system was provided by J. Xiong at the Institute of Molecular Medicine, College of Future Technology, Peking University (Beijing, China). Specifically, the green FUCCI reporter system was constructed by overexpressing a nonfunctional human Geminin deletion mutant fused to Azami Green, mAG-hGeminin (1/110), driven by the Tnnt2 promoter. During the G1 phase, geminin was ubiquitinated and degraded by proteasomes, resulting in the absence of green fluorescence in the G1 stage and the appearance of green signals in the S, G2, and M phases of the cell cycle. The green FUCCI system was packaged in an adenovirus vector for visualizing the cardiomyocytes that were in the S, G2, and M phases, as previously reported (*22*). The adenovirus packaging of pAdeno-cTNT-MAG-hegenmin was accomplished by OBiO Technology (Shanghai, China).

AAV9 injection

For AAV injection, P1 WT C57BL/6 mice were randomly assigned to receive subcutaneous injection of AAV9-*Ptma* or AAV9-*Luc* (2×10^{11} viral genome particles per mouse heart), respectively. Then, 7 days after virus injection, the mice underwent MI surgery or sham operation.

For the adult heart, intramyocardial injection of AAV9-*Ptma* or AAV9-*Luc* (5×10^{11} viral genome particles per mouse heart) following MI was performed as reported in our previous study (*21*). After MI surgery was performed, 30 μl of AAV9-*Ptma* or AAV9-*Luc* was immediately injected into the ventricle muscular wall, and the virus was evenly distributed into five sites around the infarcted area, including two sites in the anterior wall, two sites in the lateral wall, and one site in the apex area. The dissected intercostal space and chest skin were sutured with a 4-0 silk suture (Ethicon, USA), and the animal was placed in a prone position on a heating plate at 37°C until recovery of spontaneous breathing.

Virus infection and siRNA transfection

For lentivirus infection, cardiomyocytes were infected at a multiplicity of infection (MOI) of 20 to 50 in DMEM (Gibco, 11885) with no FBS for 20 to 24 hours. Then, the culture medium was replaced with DMEM containing 0.5% FBS (Gibco, 10437077) for 24 hours, and the cells were cultured under 3% O_2 to mimic MI-induced cardiomyocyte hypoxia. After that, the cardiomyocytes were harvested for Western blot, qRT-PCR, or immunofluorescence staining analysis. For EdU incorporation assay, 10 μM EdU (Invitrogen, A10044) was added to the culture medium for 24 hours after virus infection.

As for adenovirus infection, the cardiomyocytes were infected with adenovirus at an MOI of 50 to 100. The experiment was performed following the same procedure as lentivirus infection mentioned above. siRNA targeting *Ptma*, *Mbd3*, *Nsun2*, *Grwd1*, and *H2az* was designed and synthesized by GenePharma (Suzhou, China), and the targeting siRNA and scramble control were transfected into NMCMs or NRCMs at a final concentration of 50 nM using Lipofectamine RNAiMAX Reagent (Invitrogen, 13778075). The sequences of siRNAs are provided in data S3.

Immunofluorescence staining

Following virus infection or siRNA transfection, the harvested cardiomyocytes were fixed with 4% PFA (Beyotime, P0099) for 15 min, washed three times with PBS to remove residual PFA, then permeabilized with 0.5% Triton X-100, and blocked with 5% donkey serum for 1 hour at RT. After overnight incubation with the primary antibody, the cells were left at RT for 45 min before incubating with the secondary antibody. Targeting primary and secondary antibodies are provided in table S3. The Opera Phenix Plus High-Content Screening System (PerkinElmer, USA) was used for imaging and quantification of cardiomyocyte proliferation. The representative images were captured by a ZEISS LSM800 confocal laser scanning microscope (ZEISS, Germany).

EdU incorporation assay

To assess whether PTMA promoted cardiomyocyte DNA synthesis in vivo, the mice were administered EdU (Invitrogen, A10044; 5 mg/kg, intraperitoneally) as described previously (*45*), and the administration frequency was shown in the diagram of each experiment. Then, the Click-iT EdU Imaging Kit (Invitrogen, C10637) was used to detect the cells labeled with EdU according to the user manual. EdU-positive cardiomyocytes were quantified as the percentage of the total number of cardiomyocytes analyzed.

IP and co-IP

The cardiomyocytes were lysed in immunoprecipitation (IP) lysis buffer (Invitrogen, USA) containing protease inhibitor cocktail (Roche, 4693159001) for 10 min at 4°C. After the lysate was centrifuged at 13,000*g* for 10 min, the proteins in the suspension were measured with an Enhanced BCA Protein Assay Kit (Beyotime, BCP0010S). Total protein (2 mg) per IP reaction was exposed to the indicated primary antibodies at 4°C overnight with rotation, followed by the incubation with Protein G Dynabeads (Invitrogen, 88847). The incubated beads were rinsed with IP lysis buffer. Then, 100 μl of 3× SDS loading buffer (Invitrogen, B0008) was added to the beads, and the bound proteins were detached from the beads after denaturation at 95°C. The mass spectrometry was performed by Beijing Precise Health Biotechnology Co. Ltd.

Western blot analysis

For protein extraction, radioimmunoprecipitation assay (RIPA) lysis buffer (Beyotime, P0013B) supplemented with protease inhibitors was prepared for heart tissue protein extraction. The RIPA lysis buffer supplement with protease inhibitor and PhosSTOP cocktail (Sigma-Aldrich, 4693159001 and 4906837001) and 1 mM phenylmethylsulfonyl fluoride (Beyotime, ST507) was used for cardiomyocyte protein extraction. The proteins (50 μg total protein for each tissue sample) were separated by 12% or 4 to 12% NuPAGE bis-tris gel followed by iBlot 3 Western blot electrophoretic transfer systems (Thermo Fisher Scientific, Germany) or Bio-Rad Mini Trans-Blot (Bio-Rad, USA). Following blocking in 5% skimmed milk, membranes were exposed to the specified primary antibodies at 4°C overnight and rinsed with TBST buffer thrice before incubation with horseradish peroxidase–conjugated secondary antibodies for 1 hour at RT. Protein bands were detected using ECL Reagent (Invitrogen, A38556) with the Tanon imaging system (Tanon, China) or ChemiDoc MP system (Bio-Rad, USA). All the antibody information is listed in table S3.

Quantitative reverse transcription polymerase chain reaction

Total RNA from cardiomyocytes was extracted using TRIzol reagent (Invitrogen, 15596018), and, then, it was purified and converted to cDNA using HiScript II 1st Strand cDNA Synthesis Kit (+gDNA wiper) (Vazyme biotech, R212-01) following the user manual. qRT-PCR signal was measured using the Vii7 Real-time PCR System with ChamQ Universal SYBR qPCR Master Mix (Vazyme biotech, Q711-02). Gene expression was determined by ΔΔCt from qPCR datasets. Data were normalized to RN18s or Actb signal. Primers used for qRT-PCR are listed in data S3.

Bulk RNA-seq and data analysis

Total RNA from treated samples was isolated using TRIzol reagent (Invitrogen, 15596018). Then, bulk RNA library preparation and sequencing were carried out by Novogene (Beijing, China). Briefly, RNA integrity was assessed using the RNA Nano 6000 Assay Kit on the Bio-analyzer 2100 system (Agilent Technologies, CA, USA). All samples submitted for library construction had an RNA integrity number of 8 or greater, and a total amount of 1 μg RNA per sample was used for RNA sample preparations. According to the manufacturer's guidelines, library construction was performed using NEBNext Ultra RNA Library Prep Kit for Illumina (New England Biolabs, E7490). Index codes were incorporated to assign sequences to each sample. The indexed libraries were then pooled and run on the Illumina NovaSeq 6000 platform for 150–base pair (bp) paired-end sequencing.

At least 6-GB data per sample were obtained. Trimmomatic (version 0.39) was used to remove low-quality reads. After that, the clean reads were mapped to the mouse reference genome (mm10) using Hisat2 (version 2.1.0), and the expression data were obtained by featureCounts (version 2.0.0). Subsequently, the differential expression analysis was performed between the two groups using the DESeq2 R package (version 1.34.0) (*59*). The adjusted *P* values were calculated using Benjamini and Hochberg's approaches to control the false discovery rate. Genes with an adjusted *P* value less than 0.05 were identified as differentially expressed. The Gene Ontology (GO) enrichment terms were analyzed using metascape or clusterprofiler R package (version 4.2.2) (*60*). Raw reads generated for the samples have been submitted to National Center for Biotechnology Information (NCBI) based on the BioProject numbers PRJNA1102164 (RNA-seq data of cardiomyocytes treated with si-*Ptma* versus si-NC) and PRJNA1030978 (RNA-seq data of hiPSC-CMs treated with Ad-*PTMA* versus Ad-*Luc*).

WGCNA network construction and module identification

The WGCNA R package (version 1.71) was used to construct a gene-gene similarity network during cardiomyocyte development (*20*). The expression data were obtained from our previously published bulk RNA-seq data (NCBI BioProject ID: PRJNA798841) of cardiomyocytes from varied developmental periods (*19*). The cardiomyocytes were separated from mice hearts at E14.5, P1, P4, P7, P14, and P56 with three replicates per time point. After removing those genes with zero expression, 12,566 genes with a median deviation in the top 75% were selected for creating the signed gene co-expression network. The normalized gene expression was used to compute the pairwise Pearson correlation coefficients between all genes, and the weighted network adjacency was obtained using a proper soft thresholding power β, which was chosen to satisfy the scale-free topology criterion. To reduce the effects of noise and weak correlations, the adjacency matrix was then transformed into the topological overlap matrix (TOM), which measures the shared network neighborhood of each pair of genes. The network dissimilarity, defined by TOM, formed the basis for clustering genes into modules using hierarchical clustering. A total of 13 modules were obtained and assigned to different colors for identification. The gray module contains the genes that are not classified into other modules. For each module, the average gene expression across all sampling time points was calculated and graphically represented with a trend line to delineate the module's expression profile throughout the developmental timeline. Correlation analysis with external traits, such as cardiomyocyte proliferation, was conducted on each module. Modules with high correlation coefficient and adjusted *P* value < 0.05 may be related to cardiomyocyte proliferation. For the module blue, the MM was calculated

for each gene, which reflects the intramodular importance and connectivity. The GS value was also computed to quantify the association of individual genes with cardiomyocyte proliferation. Genes with high GS value and high intramodular connectivity in the blue module were considered hub genes (MM > 0.95, GS > 0.75, and adjusted P value < 0.05 for MM and GS).

scRNA-seq preparation

Embryonic hearts were collected from various developmental periods including E8.5, E9.0, E9.5, E10.5, E11.5, E14.5, and E17.5. Biological replicates were set for the hearts from E9.0 to E10.5. E8.5 to E10.5 heart tissues were cut into small pieces in prechilled PBS and digested with 0.25% trypsin-EDTA (Gibco, 25200056) incubated in a 37°C water bath with mild shaking, while E11.5-E17.5 cardiac cells were isolated using the Neonatal Heart Dissociation Kit in combination with gentle MACS and Octo Dissociator (Miltenyi BioTec, Teterow, Germany). The cell counts and vitality were then verified by the Countstar cell analyzer.

Single-cell library construction and sequencing

scRNA-seq library preparation and sequencing were conducted by BoAo (Beijing, China) using Single Cell 3′ V2 Reagent Kit according to the protocol of the manufacturer. Briefly, cells were loaded to generate Gel Bead-In-Emulsions (GEMs). Subsequently, the cells underwent lysis, followed by reverse transcription within the GEMs. The cDNA was then amplified by PCR for 14 cycles, after which the GEMs were broken. The amplified cDNA was further subjected to purification and size selection. Following fragmentation and end-repair, the cDNA fragments were ligated with adapters, sample indices, and sequencing primers. Subsequently, the libraries were purified and quantified to ensure that they met the required standards for sequencing. After quality control, the libraries were sequenced on Illumina XT10, and 150-bp paired-end sequencing reads were generated. Raw data of scRNA-seq have been deposited under the accession number CRA002015 in the Beijing Institute of Genomics Data Center.

scRNA-seq data analysis

The raw data were aligned to the mouse mm10 transcriptome using CellRanger (version 4.0.0, 10× Genomics). The subsequent analysis, including quality control, unsupervised clustering, and differential gene expression analysis, was implemented using the Seurat R package (version 4.0.5). In the quality control process, the filter conditions of nFeature_RNA and nCount_RNA were set separately to remove the outliers according to the distribution of each sample. Cells with mitochondrial content less than 20% were retained. The doublets identified by DoubletFinder were then removed (*61*). After the above processing, 10 samples were combined and normalized by SCTransform to achieve a negative binomial distribution with the mitochondrial percentage regressed out. Then, the Harmony R package (0.1.0) was used to generate 50 harmonized dimension reduction components, and the top 30 harmony dimensions were selected for clustering analysis. The t-SNE projections were then computed for visualization. Clusters were annotated on the basis of SingleR and the expression of known marker genes. Differentially expressed genes in each cluster were calculated using the FindAllMarkers function. Genes with FC > 1.2, adjusted P value < 0.05, and expression percentage of VCM1 > 0.9 were considered the highly expressed genes of VCM1. GO analysis was performed with metascape.

The CellCycleScoring function was used to calculate cell cycle scores for each cell. It used a gene set enrichment analysis approach to infer cell cycle activity based on the expression levels of known cell cycle marker genes. The function first identified the S and G_2-M phase marker genes by intersecting the provided gene lists (S genes and G_2-M genes) with the genes present in the Seurat object. Then, it calculated the average expression of the S phase genes and the G_2-M phase genes for each cell.

Statistical analysis

The analyses of animal experiments were performed in a double-blind fashion. Statistical analysis and plotting were performed using GraphPad Prism version 8.2.1 (GraphPad Software Inc., San Diego, CA). The Brown-Forsythe test was applied to test the equality of variances. When comparing the statistical significance between two groups, a two-tailed Student's t test was applied for the data with homogeneous variance, and the Mann-Whitney test was applied for the data with heterogeneous variance. When comparing more than two groups, one-way or two-way analysis of variance (ANOVA) was performed followed by the Šidák or Tukey multiple comparisons test. Unless otherwise stated, all data are presented as the means ± SEM. The results with P value < 0.05 were considered statistically significant and the value of n is mentioned in the figure legends.

Supplementary Materials

The PDF file includes:

Figs. S1 to S6
Tables S1 to S4
Legends for datasets S1 to S3

Other Supplementary Material for this manuscript includes the following:

Datasets S1 to S3

REFERENCES AND NOTES

1. A. N. Nowbar, M. Gitto, J. P. Howard, D. P. Francis, R. Al-Lamee, Mortality from ischemic heart disease. *Circ. Cardiovasc. Qual. Outcomes* **12**, e005375 (2019).
2. F. Zhu, Q. Meng, Y. Yu, L. Shao, Z. Shen, Adult cardiomyocyte proliferation: A new insight for myocardial infarction therapy. *J. Cardiovasc. Transl. Res.* **14**, 457–466 (2021).
3. B. A. French, C. M. Kramer, Mechanisms of post-infarct left ventricular remodeling. *Drug Discov. Today Dis. Mech.* **4**, 185–196 (2007).
4. M. A. Konstam, D. G. Kramer, A. R. Patel, M. S. Maron, J. E. Udelson, Left ventricular remodeling in heart failure: Current concepts in clinical significance and assessment. *JACC Cardiovasc. Imaging* **4**, 98–108 (2011).
5. Y. Barak, M. Hemberger, H. M. Sucov, Phases and mechanisms of embryonic cardiomyocyte proliferation and ventricular wall morphogenesis. *Pediatr. Cardiol.* **40**, 1359–1366 (2019).
6. C. M. J. Tan, A. J. Lewandowski, The transitional heart: From early embryonic and fetal development to neonatal life. *Fetal Diagn. Ther.* **47**, 373–386 (2020).
7. A. C. Sturzu, K. Rajarajan, D. Passer, K. Plonowska, A. Riley, T. C. Tan, A. Sharma, A. F. Xu, M. C. Engels, R. Feistritzer, G. Li, M. K. Selig, R. Geissler, K. D. Robertson, M. Scherrer-Crosbie, I. J. Domian, S. M. Wu, Fetal mammalian heart generates a robust compensatory response to cell loss. *Circulation* **132**, 109–121 (2015).
8. Z. Wang, M. Cui, A. M. Shah, W. Ye, W. Tan, Y.-L. Min, G. A. Botten, J. M. Shelton, N. Liu, R. Bassel-Duby, E. N. Olson, Mechanistic basis of neonatal heart regeneration revealed by transcriptome and histone modification profiling. *Proc. Natl. Acad. Sci. U.S.A.* **116**, 18455–18465 (2019).
9. D. M. Bryant, C. C. O'Meara, N. N. Ho, J. Gannon, L. Cai, R. T. Lee, A systematic analysis of neonatal mouse heart regeneration after apical resection. *J. Mol. Cell. Cardiol.* **79**, 315–318 (2015).
10. E. R. Porrello, A. I. Mahmoud, E. Simpson, J. A. Hill, J. A. Richardson, E. N. Olson, H. A. Sadek, Transient regenerative potential of the neonatal mouse heart. *Science* **331**, 1078–1080 (2011).
11. F. Li, X. Wang, J. M. Capasso, A. M. Gerdes, Rapid transition of cardiac myocytes from hyperplasia to hypertrophy during postnatal development. *J. Mol. Cell. Cardiol.* **28**, 1737–1746 (1996).

12. Z. Karetsou, R. Sandaltzopoulos, M. Frangou-Lazaridis, C. Y. Lai, O. Tsolas, P. B. Becker, T. Papamarcaki, Prothymosin α modulates the interaction of histone H1 with chromatin. *Nucleic Acids Res.* **26**, 3111–3118 (1998).
13. K. P. Letsas, M. Frangou-Lazaridis, Surfing on prothymosin α proliferation and anti-apoptotic properties. *Neoplasma* **53**, 92–96 (2006).
14. A. Cannavo, G. Rengo, D. Liccardo, G. Pironti, M. C. Scimia, L. Scudiero, C. De Lucia, M. Ferrone, D. Leosco, N. Zambrano, W. J. Koch, B. Trimarco, G. Esposito, Prothymosin α protects cardiomyocytes against ischemia-induced apoptosis via preservation of Akt activation. *Apoptosis* **18**, 1252–1261 (2013).
15. J. Gomez-Marquez, P. Rodríguez, Prothymosin α is a chromatin-remodelling protein in mammalian cells. *Biochem. J.* **333** (Pt 1), 1–3 (1998).
16. Z. Karetsou, G. Martic, S. Tavoulari, S. Christoforidis, M. Wilm, C. Gruss, T. Papamarcaki, Prothymosin α associates with the oncoprotein SET and is involved in chromatin decondensation. *FEBS Lett.* **577**, 496–500 (2004).
17. K. Vareli, M. Frangou-Lazaridis, Prothymosin α is localized in mitotic spindle during mitosis. *Biol. Cell* **96**, 421–428 (2004).
18. M. S. Kowalczyk, I. Tirosh, D. Heckl, T. N. Rao, A. Dixit, B. J. Haas, R. K. Schneider, A. J. Wagers, B. L. Ebert, A. Regev, Single-cell RNA-seq reveals changes in cell cycle and differentiation programs upon aging of hematopoietic stem cells. *Genome Res.* **25**, 1860–1872 (2015).
19. J. Feng, Y. Li, Y. Nie, Methods of mouse cardiomyocyte isolation from postnatal heart. *J. Mol. Cell. Cardiol.* **168**, 35–43 (2022).
20. P. Langfelder, S. Horvath, WGCNA: An R package for weighted correlation network analysis. *BMC Bioinformatics* **9**, 559 (2008).
21. N. Liu, M. Kataoka, Y. Wang, L. Pu, X. Dong, X. Fu, F. Zhang, F. Gao, T. Liang, J. Pei, C. Xiao, Q. Qiu, T. Hong, Q. Chen, J. Zhao, L. Zhu, J. He, X. Hu, Y. Nie, W. Zhu, H. Yu, D. B. Cowan, X. Hu, J. Wang, D.-Z. Wang, J. Chen, LncRNA *LncHrt* preserves cardiac metabolic homeostasis and heart function by modulating the LKB1-AMPK signaling pathway. *Basic Res. Cardiol.* **116**, 48 (2021).
22. J. Du, L. Zheng, P. Gao, H. Yang, W.-J. Yang, F. Guo, R. Liang, M. Feng, Z. Wang, Z. Zhang, L. Bai, Y. Bu, S. Xing, W. Zheng, X. Wang, L. Quan, X. Hu, H. Wu, Z. Chen, L. Chen, K. Wei, Z. Zhang, X. Zhu, X. Zhang, Q. Tu, S.-M. Zhao, X. Lei, J.-W. Xiong, A small-molecule cocktail promotes mammalian cardiomyocyte proliferation and heart regeneration. *Cell Stem Cell* **29**, 545–558.e13 (2022).
23. T. Liang, F. Gao, J. Jiang, Y. W. Lu, F. Zhang, Y. Wang, N. Liu, X. Fu, X. Dong, J. Pei, D. B. Cowan, X. Hu, J. Wang, D.-Z. Wang, J. Chen, Loss of phosphatase and tensin homolog promotes cardiomyocyte proliferation and cardiac repair after myocardial infarction. *Circulation* **142**, 2196–2199 (2020).
24. Z. Lin, A. von Gise, P. Zhou, F. Gu, Q. Ma, J. Jiang, A. L. Yau, J. N. Buck, K. A. Gouin, P. R. R. van Gorp, B. Zhou, J. Chen, J. G. Seidman, D.-Z. Wang, W. T. Pu, Cardiac-specific YAP activation improves cardiac function and survival in an experimental murine MI model. *Circ. Res.* **115**, 354–363 (2014).
25. L. Morey, C. Brenner, F. Fazi, R. Villa, A. Gutierrez, M. Buschbeck, C. Nervi, S. Minucci, F. Fuks, L. Di Croce, MBD3, a component of the NuRD complex, facilitates chromatin alteration and deposition of epigenetic marks. *Mol. Cell. Biol.* **28**, 5912–5923 (2008).
26. N. Mor, Y. Rais, D. Sheban, S. Peles, A. Aguilera-Castrejon, A. Zviran, D. Elinger, S. Viukov, S. Geula, V. Krupalnik, M. Zerbib, E. Chomsky, L. Lasman, T. Shani, J. Bayerl, O. Gafni, S. Hanna, J. D. Buenrostro, T. Hagai, H. Masika, G. Vainorius, Y. Bergman, W. J. Greenleaf, M. A. Esteban, U. Elling, Y. Levin, R. Massarwa, Y. Merbl, N. Novershtern, J. H. Hanna, Neutralizing Gatad2a-Chd4-Mbd3/NuRD complex facilitates deterministic induction of naive pluripotency. *Cell Stem Cell* **23**, 412–425.e10 (2018).
27. M. L. Amaya, A. Inguva, S. Pei, C. Jones, A. Krug, H. Ye, M. Minhajuddin, A. Winters, S. L. Furtek, F. Gamboni, B. Stevens, A. D'Alessandro, D. A. Pollyea, P. Reigan, C. T. Jordan, The STAT3-MYC axis promotes survival of leukemia stem cells by regulating SLC1A5 and oxidative phosphorylation. *Blood* **139**, 584–596 (2022).
28. J.-L. Lee, M.-J. Wang, J.-Y. Chen, Acetylation and activation of STAT3 mediated by nuclear translocation of CD44. *J. Cell Biol.* **185**, 949–957 (2009).
29. Z.-L. Yuan, Y.-J. Guan, D. Chatterjee, Y. E. Chin, Stat3 dimerization regulated by reversible acetylation of a single lysine residue. *Science* **307**, 269–273 (2005).
30. Y. Li, J. Feng, S. Song, H. Li, H. Yang, B. Zhou, Y. Li, Z. Yue, H. Lian, L. Liu, S. Hu, Y. Nie, gp130 controls cardiomyocyte proliferation and heart regeneration. *Circulation* **142**, 967–982 (2020).
31. L. Zhuang, K. Jia, C. Chen, Z. Li, J. Zhao, J. Hu, H. Zhang, Q. Fan, C. Huang, H. Xie, L. Lu, W. Shen, G. Ning, J. Wang, R. Zhang, K. Chen, X. Yan, DYRK1B-STAT3 drives cardiac hypertrophy and heart failure by impairing mitochondrial bioenergetics. *Circulation* **145**, 829–846 (2022).
32. J. Grego-Bessa, L. Luna-Zurita, G. del Monte, V. Bolós, P. Melgar, A. Arandilla, A. N. Garratt, H. Zang, Y.-S. Mukouyama, H. Chen, W. Shou, E. Ballestar, M. Esteller, A. Rojas, J. M. Pérez-Pomares, J. L. de la Pompa, Notch signaling is essential for ventricular chamber development. *Dev. Cell* **12**, 415–429 (2007).
33. M. J. Bywater, D. L. Burkhart, J. Straube, A. Sabò, V. Pendino, J. E. Hudson, G. A. Quaife-Ryan, E. R. Porrello, J. Rae, R. G. Parton, T. R. Kress, B. Amati, T. D. Littlewood, G. I. Evan, C. H. Wilson, Reactivation of Myc transcription in the mouse heart unlocks its proliferative capacity. *Nat. Commun.* **11**, 1827 (2020).
34. D. E. Ebeid, F. Firouzi, C. Y. Esquer, J. M. Navarrete, B. J. Wang, N. A. Gude, M. A. Sussman, PIM1 promotes survival of cardiomyocytes by upregulating c-Kit protein expression. *Cells* **9**, 2001 (2020).
35. L. Nežić, R. Škrbić, L. Amidžić, R. Gajanin, K. Kuča, V. Jaćević, Simvastatin protects cardiomyocytes against endotoxin-induced apoptosis and up-regulates survivin/NF-κB/p65 expression. *Sci. Rep.* **8**, 14652 (2018).
36. A. Wu, C. Zhong, X. Song, W. Yuan, M. Tang, T. Shu, H. Huang, P. Yang, Q. Liu, The activation of LBH-CRYAB signaling promotes cardiac protection against I/R injury by inhibiting apoptosis and ferroptosis. *iScience* **27**, 109510 (2024).
37. M. Toyoda, H. Shirato, K. Nakajima, M. Kojima, M. Takahashi, M. Kubota, R. Suzuki-Migishima, Y. Motegi, M. Yokoyama, T. Takeuchi, *jumonji* downregulates cardiac cell proliferation by repressing *cyclin D1* expression. *Dev. Cell* **5**, 85–97 (2003).
38. H. Ueda, K. Sasaki, S. K. Halder, Y. Deguchi, K. Takao, T. Miyakawa, A. Tajima, Prothymosin α-deficiency enhances anxiety-like behaviors and impairs learning/memory functions and neurogenesis. *J. Neurochem.* **141**, 124–136 (2017).
39. A. Emmanouilidou, Z. Karetsou, E. Tzima, T. Kobayashi, T. Papamarcaki, Knockdown of prothymosin α leads to apoptosis and developmental defects in zebrafish embryos. *Biochem. Cell Biol.* **91**, 325–332 (2013).
40. M. M. Gladka, A. K. Z. Johansen, S. J. van Kampen, M. M. C. Peters, B. Molenaar, D. Versteeg, L. Kooijman, L. Zentilin, M. Giacca, E. van Rooij, Thymosin β4 and prothymosin alpha promote cardiac regeneration post-ischaemic injury in mice. *Cardiovasc. Res.* **119**, 802–812 (2023).
41. A.-L. Shiau, S.-Y. Fang, C.-H. Hsu, M.-H. Chiu, C.-F. Lam, C.-L. Wu, J. N. Roan, Prothymosin α gene transfer modulates myocardial remodeling after ischemia-reperfusion injury. *Acta Cardiol. Sin.* **38**, 187–200 (2022).
42. M. M. Gladka, A. Kohela, B. Molenaar, D. Versteeg, L. Kooijman, J. Monshouwer-Kloots, V. Kremer, H. R. Vos, M. M. H. Huibers, J. J. Haigh, D. Huylebroeck, R. A. Boon, M. Giacca, E. van Rooij, Cardiomyocytes stimulate angiogenesis after ischemic injury in a ZEB2-dependent manner. *Nat. Commun.* **12**, 84 (2021).
43. E. M. George, D. T. Brown, Prothymosin α is a component of a linker histone chaperone. *FEBS Lett.* **584**, 2833–2836 (2010).
44. G. Covelo, C. S. Sarandeses, C. Díaz-Jullien, M. Freire, Prothymosin alpha interacts with free core histones in the nucleus of dividing cells. *J. Biochem.* **140**, 627–637 (2006).
45. K. Kaji, J. Nichols, B. Hendrich, Mbd3, a component of the NuRD co-repressor complex, is required for development of pluripotent cells. *Development* **134**, 1123–1132 (2007).
46. J. Basta, M. Rauchman, The nucleosome remodeling and deacetylase complex in development and disease. *Transl. Res.* **165**, 36–47 (2015).
47. C. J. Millard, N. Varma, A. Saleh, K. Morris, P. J. Watson, A. R. Bottrill, L. Fairall, C. J. Smith, J. W. Schwabe, The structure of the core NuRD repression complex provides insights into its interaction with chromatin. *eLife* **5**, e13941 (2016).
48. N. Reynolds, P. Latos, A. Hynes-Allen, R. Loos, D. Leaford, A. O'Shaughnessy, O. Mosaku, J. Signolet, P. Brennecke, T. Kalkan, I. Costello, P. Humphreys, W. Mansfield, K. Nakagawa, J. Strouboulis, A. Behrens, P. Bertone, B. Hendrich, NuRD suppresses pluripotency gene expression to promote transcriptional heterogeneity and lineage commitment. *Cell Stem Cell* **10**, 583–594 (2012).
49. C. Han, Y. Nie, H. Lian, R. Liu, F. He, H. Huang, S. Hu, Acute inflammation stimulates a regenerative response in the neonatal mouse heart. *Cell Res.* **25**, 1137–1151 (2015).
50. G. Wei, C. Li, X. Jia, J. Xie, Z. Tang, M. Jin, Q. Chen, Y. Sun, S. He, X. Li, Y. Chen, H. Zheng, W. Liao, Y. Liao, J. Bin, S. Huang, Extracellular vesicle-derived CircWhsc1 promotes cardiomyocyte proliferation and heart repair by activating TRIM59/STAT3/Cyclin B2 pathway. *J. Adv. Res.* **53**, 199–218 (2023).
51. Y. Fang, V. Gupta, R. Karra, J. E. Holdway, K. Kikuchi, K. D. Poss, Translational profiling of cardiomyocytes identifies an early Jak1/Stat3 injury response required for zebrafish heart regeneration. *Proc. Natl. Acad. Sci. U.S.A.* **110**, 13416–13421 (2013).
52. K. Leslie, C. Lang, G. Devgan, J. Azare, M. Berishaj, W. Gerald, Y. B. Kim, K. Paz, J. E. Darnell, C. Albanese, T. Sakamaki, R. Pestell, J. Bromberg, Cyclin D1 is transcriptionally regulated by and required for transformation by activated signal transducer and activator of transcription 3. *Cancer Res.* **66**, 2544–2552 (2006).
53. Y. Ye, K. Yang, H. Liu, Y. Yu, M. Song, D. Huang, J. Lei, Y. Zhang, Z. Liu, Q. Chu, Y. Fan, S. Zhang, Y. Jing, C. R. Esteban, S. Wang, J. C. I. Belmonte, J. Qu, W. Zhang, G.-H. Liu, SIRT2 counteracts primate cardiac aging via deacetylation of STAT3 that silences CDKN2B. *Nat. Aging* **3**, 1269–1287 (2023).
54. S. Kleinsimon, E. Longmuss, J. Rolff, S. Jäger, A. Eggert, C. Delebinski, G. Seifert, GADD45A and CDKN1A are involved in apoptosis and cell cycle modulatory effects of viscumTT with further inactivation of the STAT3 pathway. *Sci. Rep.* **8**, 5750 (2018).
55. J. Feng, Y. Li, Y. Li, Q. Yin, H. Li, J. Li, B. Zhou, J. Meng, H. Lian, M. Wu, Y. Li, K. Dou, W. Song, B. Lu, L. Liu, S. Hu, Y. Nie, Versican promotes cardiomyocyte proliferation and cardiac repair. *Circulation* **149**, 1004–1015 (2024).
56. F. Gao, M. Kataoka, N. Liu, T. Liang, Z.-P. Huang, F. Gu, J. Ding, J. Liu, F. Zhang, Q. Ma, Y. Wang, M. Zhang, X. Hu, J. Kyselovic, X. Hu, W. T. Pu, J. Wang, J. Chen, D.-Z. Wang,

Therapeutic role of miR-19a/19b in cardiac regeneration and protection from myocardial infarction. *Nat. Commun.* **10**, 1802 (2019).
57. N. U. N. Nguyen, D. C. Canseco, F. Xiao, Y. Nakada, S. Li, N. T. Lam, S. A. Muralidhar, J. J. Savla, J. A. Hill, V. Le, K. A. Zidan, H. W. El-Feky, Z. Wang, M. S. Ahmed, M. E. Hubbi, I. Menendez-Montes, J. Moon, S. R. Ali, V. Le, E. Villalobos, M. S. Mohamed, W. M. Elhelaly, S. Thet, C. G. Anene-Nzelu, W. L. W. Tan, R. S. Foo, X. Meng, M. Kanchwala, C. Xing, J. Roy, M. S. Cyert, B. A. Rothermel, H. A. Sadek, A calcineurin-Hoxb13 axis regulates growth mode of mammalian cardiomyocytes. *Nature* **582**, 271–276 (2020).
58. D. Cai, C. Liu, H. Li, C. Wang, L. Bai, J. Feng, M. Hu, H. Wang, S. Song, Y. Xie, Z. Chen, J. Zhong, H. Lian, Z. Yang, Y. Zhang, Y. Nie, Foxk1 and Foxk2 promote cardiomyocyte proliferation and heart regeneration. *Nat. Commun.* **16**, 2877 (2025).
59. M. I. Love, W. Huber, S. Anders, Moderated estimation of fold change and dispersion for RNA-seq data with DESeq2. *Genome Biol.* **15**, 550 (2014).
60. Y. Zhou, B. Zhou, L. Pache, M. Chang, A. H. Khodabakhshi, O. Tanaseichuk, C. Benner, S. K. Chanda, Metascape provides a biologist-oriented resource for the analysis of systems-level datasets. *Nat. Commun.* **10**, 1523 (2019).
61. C. S. McGinnis, L. M. Murrow, Z. J. Gartner, DoubletFinder: Doublet detection in single-cell RNA sequencing data using artificial nearest neighbors. *Cell Syst.* **8**, 329–337.e4 (2019).

Acknowledgments: We thank J. Chen at Zhejiang University for providing the lineage tracing *Myh6-MerCreMer* mice with a loxP-flanked multicolor fluorescent protein confetti mouse line and J. Xiong from Peking University for providing FUCCI plasmid pAdeno-Tnnt2-mAG-hGeminin (1/110). Schematic was created with BioRender.com. **Funding:** This work was supported by the National Natural Science Foundation of China (NSFC) (82425006 to Y.N., 82400355 to N.L., and 82300301 to J.P.), the Chinese Academy of Medical Sciences (CAMS) Innovation Fund for Medical Sciences (CAMS-I2M, 2024-I2M-TS-003 to Y.N.), the National Key Research and Development Project of China (2022YFA1104503 to Y.N.), Non-profit Central Research Institute Fund of Chinese Academy of Medical Sciences (2024-RC320-04 and 2023-PT310-03 to Y.N.), and National High Level Hospital Clinical Research Funding (2023-GSP-ZD-2-01 to Y.N.). **Author contributions:** Conceptualization: Y.N. Data curation: N.L. and Y. X. Formal analysis: N.L., J.P., Y.X., and X.L. Funding acquisition: Y.N. and N.L. Investigation: N.L., J.P., Y.X., H.X., N.J., J.W., Y.G., Y.L., W.L., C.X., Z.Q., and H.C. Methodology: N.L., J.P., Y.X., H.X., N.J., J.W., Y.L., W.L., C.X., and Z.Q. Project administration: Y.N. and N.L. Resources: N.L. and X.L. Software: Y.X. and X.L. Supervision: Y.N. and N.L. Validation: Y.N., N.L., J.P., Y.X., J.W., and Y.G. Visualization: N.L., J.P., Y.X., and X.L. Writing—original draft: N.L., J.P., and Y.X. Writing—review and editing: Y.N., N.L., J.P., and Y.X. **Competing interests:** Y.N. and N.L. declared a patent related to cardiac repair by PTMA coding sequence, and the patent application related to this work has been submitted. The other authors declare that they have no competing interests. **Data and materials availability:** All data needed to evaluate the conclusions in the paper are present in the paper and/or the Supplementary Materials. Raw data of the related next generation sequencing are available from Beijing Institute of Genomics Data Center (accession: CRA002015, scRNA-seq data of mouse embryonic hearts) and National Center for Biotechnology Information (accession: PRJNA1102164, RNA-seq data of cardiomyocytes treated with si-*Ptma* versus si-NC; and accession: PRJNA1030978, RNA-seq data of hiPSC-CMs treated with Ad-*PTMA* versus Ad-*Luc*).

Submitted 21 October 2024
Accepted 18 April 2025
Published 23 May 2025
10.1126/sciadv.adt9446